ϵ-site cleavages do not always correlate (*17*). Furthermore, in the current study, we showed that the precision of ϵ- and γ-site cleavages on PM and endosomes did not change in parallel. Our results support the hypothesis that the ϵ-cleavage process is distinct from that of the γ-cleavage, although both occur on the same transmembrane domain and are mediated by the same PS-dependent γ-secretases.

Recent reports have described the existence of several long Aβ species that are thought to be membrane-bound remnants from ϵ-cleavage of CTF stubs (*35*−*37*). Also, it has been reported that there is an association between the cleavages at ϵ51 and at γ42, which are types of ϵ- and γ-site cleavages, respectively (*16*). These findings indicate that there is a time-dependent relationship between γ- and ϵ-cleavages, namely, that γ-cleavage follows ϵ-cleavage (*36*, *37*). If this is generally true, de novo AICD and Aβ is generated from distinct substrates in our cell-free assay; in other words, AICDs is generated from CTF stubs of βAPP, whereas Aβ must be generated from long and membrane-bound Aβ. Otherwise, our results suggest that the process determining the precision of ϵ-cleavage is distinct from that for the γ-cleavage. Thus, it appears that the time-dependent association between γ- and ϵ-cleavages either is not dominant but rather simply reflects the rate of each cleavage under physiological conditions.

In our cell-free assay, conditions mimicking physiological cell functions (i.e., changes in subcellular location, endocytosis, and pH) affected the efficiency of cleavage at ϵ49 and ϵ51; however, we could not find any consistent correlations between relative peak heights of AICDϵ48 and those of AICDϵ49 or AICDϵ51, even though AICDϵ48 was one of the major species.

In summary, we demonstrate here that the precision of ϵ-cleavage of βAPP changes depending on endocytotic function. In future studies, we will examine whether similar changes in the precision of PS-mediated cleavage in the TM-C also occur for other substrates, such as Notch-1.

ACKNOWLEDGMENT

We thank Drs. Harald Steiner, Masaki Nishimura, Maho Morishima-Kawashima, and Yasuo Ihara for critically reading the manuscript. We also thank Drs. Sandra L. Schmid and Takeshi Baba for providing Dyn-1 K44A-expressing HeLa cells.

SUPPORTING INFORMATION AVAILABLE

Four figures indicating that (i) inhibition of endocytosis by bafilomycin A1 treatment caused a drastic change of ϵ-cleavage precision, (ii) the relative ratio of the AICDϵ49 peak height to that of AICDϵ51 semiquantitatively correlated with the relative amount of each AICD species, and (iii) wt βAPP as well as βAPP sw caused the drastic change in the precision of ϵ-cleavage. This material is available free of charge via the Internet at http://pubs.acs.org.

REFERENCES

1. Selkoe, D., and Kopan, R. (2003) Notch and presenilin: regulated intramembrane proteolysis links development and degeneration, *Annu. Rev. Neurosci. 26*, 565−597.
2. Haass, C. (2004) Take five-BACE and the gamma-secretase quartet conduct Alzheimer's amyloid beta-peptide generation, *EMBO J. 23*, 483−488.
3. Okochi, M., Steiner, H., Fukumori, A., Tanii, H., Tomita, T., Tanaka, T., Iwatsubo, T., Kudo, T., Takeda, M., and Haass, C. (2002) Presenilins mediate a dual intramembranous gamma-secretase cleavage of Notch-1, *EMBO J. 21*, 5408−5416.
4. Lammich, S., Okochi, M., Takeda, M., Kaether, C., Capell, A., Zimmer, A. K., Edbauer, D., Walter, J., Steiner, H., and Haass, C. (2002) Presenilin-dependent intramembrane proteolysis of CD44 leads to the liberation of its intracellular domain and the secretion of an Abeta-like peptide, *J. Biol. Chem. 277*, 44754−44759.
5. Okochi, M., Fukumori, A., Jiang, J., Itoh, N., Kimura, R., Steiner, H., Haass, C., Tagami, S., and Takeda, M. (2006) Secretion of the Notch-1 Abeta-like peptide during Notch signaling, *J. Biol. Chem.* (in press).
6. Sastre, M., Steiner, H., Fuchs, K., Capell, A., Multhaup, G., Condron, M. M., Teplow, D. B., and Haass, C. (2001) Presenilin-dependent gamma-secretase processing of beta-amyloid precursor protein at a site corresponding to the S3 cleavage of Notch, *EMBO Rep. 2*, 835−841.
7. Chen, F., Gu, Y., Hasegawa, H., Ruan, X., Arawaka, S., Fraser, P., Westaway, D., Mount, H., and St George-Hyslop, P. (2002) Presenilin 1 mutations activate gamma 42-secretase but reciprocally inhibit epsilon-secretase cleavage of amyloid precursor protein (APP) and S3-cleavage of notch, *J. Biol. Chem. 277*, 36521−36526.
8. Yu, C., Kim, S. H., Ikeuchi, T., Xu, H., Gasparini, L., Wang, R., and Sisodia, S. S. (2001) Characterization of a presenilin-mediated amyloid precursor protein carboxyl-terminal fragment gamma. Evidence for distinct mechanisms involved in gamma-secretase processing of the APP and Notch1 transmembrane domains, *J. Biol. Chem. 276*, 43756−43760.
9. Gu, Y., Misonou, H., Sato, T., Dohmae, N., Takio, K., and Ihara, Y. (2001) Distinct intramembrane cleavage of the beta-amyloid precursor protein family resembling gamma-secretase-like cleavage of Notch, *J. Biol. Chem. 276*, 35235−35238.
10. Weidemann, A., Eggert, S., Reinhard, F. B., Vogel, M., Paliga, K., Baier, G., Masters, C. L., Beyreuther, K., and Evin, G. (2002) A novel epsilon-cleavage within the transmembrane domain of the Alzheimer amyloid precursor protein demonstrates homology with Notch processing, *Biochemistry 41*, 2825−2835.
11. Selkoe, D. J. (2001) Alzheimer's disease: genes, proteins, and therapy, *Physiol. Rev. 81*, 741−766.
12. Weggen, S., Eriksen, J. L., Das, P., Sagi, S. A., Wang, R., Pietrzik, C. U., Findlay, K. A., Smith, T. E., Murphy, M. P., Bulter, T., Kang, D. E., Marquez-Sterling, N., Golde, T. E., and Koo, E. H. (2001) A subset of NSAIDs lower amyloidogenic Abeta42 independently of cyclooxygenase activity, *Nature 414*, 212−216.
13. Kukar, T., Murphy, M. P., Eriksen, J. L., Sagi, S. A., Weggen, S., Smith, T. E., Ladd, T., Khan, M. A., Kache, R., Beard, J., Dodson, M., Merit, S., Ozols, V. V., Anastasiadis, P. Z., Das, P., Fauq, A., Koo, E. H., and Golde, T. E. (2005) Diverse compounds mimic Alzheimer disease-causing mutations by augmenting Abeta42 production, *Nat. Med. 11*, 545−550.
14. Lazarov, O., Robinson, J., Tang, Y. P., Hairston, I. S., Korade-Mirnics, Z., Lee, V. M., Hersh, L. B., Sapolsky, R. M., Mirnics, K., and Sisodia, S. S. (2005) Environmental enrichment reduces Abeta levels and amyloid deposition in transgenic mice, *Cell 120*, 701−713.
15. Sato, T., Dohmae, N., Qi, Y., Kakuda, N., Misonou, H., Mitsumori, R., Maruyama, H., Koo, E. H., Haass, C., Takio, K., Morishima-Kawashima, M., Ishiura, S., and Ihara, Y. (2003) Potential link between amyloid beta-protein 42 and C-terminal fragment gamma 49−99 of beta-amyloid precursor protein, *J. Biol. Chem. 278*, 24294−24301.
16. Funamoto, S., Morishima-Kawashima, M., Tanimura, Y., Hirotani, N., Saido, T. C., and Ihara, Y. (2004) Truncated carboxyl-terminal fragments of beta-amyloid precursor protein are processed to amyloid beta-proteins 40 and 42, *Biochemistry 43*, 13532−13540.
17. Moehlmann, T., Winkler, E., Xia, X., Edbauer, D., Murrell, J., Capell, A., Kaether, C., Zheng, H., Ghetti, B., Haass, C., and Steiner, H. (2002) Presenilin-1 mutations of leucine 166 equally affect the generation of the Notch and APP intracellular domains independent of their effect on Abeta 42 production, *Proc. Natl. Acad. Sci. U.S.A. 99*, 8025−8030.
18. Iwatsubo, T. (2004) The gamma-secretase complex: machinery for intramembrane proteolysis, *Curr. Opin. Neurobiol. 14*, 379−383.
19. Yu, G., Nishimura, M., Arawaka, S., Levitan, D., Zhang, L., Tandon, A., Song, Y. Q., Rogaeva, E., Chen, F., Kawarai, T.,

Supala, A., Levesque, L., Yu, H., Yang, D. S., Holmes, E., Milman, P., Liang, Y., Zhang, D. M., Xu, D. H., Sato, C., Rogaev, E., Smith, M., Janus, C., Zhang, Y., Aebersold, R., Farrer, L. S., Sorbi, S., Bruni, A., Fraser, P., and St. George-Hyslop, P. (2000) Nicastrin modulates presenilin-mediated notch/glp-1 signal transduction and betaAPP processing, *Nature 407*, 48−54.

20. Francis, R., McGrath, G., Zhang, J., Ruddy, D. A., Sym, M., Apfeld, J., Nicoll, M., Maxwell, M., Hai, B., Ellis, M. C., Parks, A. L., Xu, W., Li, J., Gurney, M., Myers, R. L., Himes, C. S., Hiebsch, R., Ruble, C., Nye, J. S., and Curtis, D. (2002) aph-1 and pen-2 are required for Notch pathway signaling, gamma-secretase cleavage of betaAPP, and presenilin protein accumulation, *Dev. Cell 3*, 85−97.
21. Wilson, C. A., Doms, R. W., Zheng, H., and Lee, V. M. (2002) Presenilins are not required for A beta 42 production in the early secretory pathway, *Nat. Neurosci. 5*, 849−855.
22. Lai, M. T., Crouthamel, M. C., DiMuzio, J., Pietrak, B. L., Donoviel, D. B., Bernstein, A., Gardell, S. J., Li, Y. M., and Hazuda, D. (2006) A presenilin-independent aspartyl protease prefers the gamma-42 site cleavage, *J. Neurochem. 96*, 118−125.
23. Okochi, M., Ishii, K., Usami, M., Sahara, N., Kametani, F., Tanaka, K., Fraser, P. E., Ikeda, M., Saunders, A. M., Hendriks, L., Shoji, S. I., Nee, L. E., Martin, J. J., Van Broeckhoven, C., St. George-Hyslop, P. H., Roses, A. D., and Mori, H. (1997) Proteolytic processing of presenilin-1 (PS-1) is not associated with Alzheimer's disease with or without PS-1 mutations, *FEBS Lett. 418*, 162−166.
24. Okochi, M., Eimer, S., Bottcher, A., Baumeister, R., Romig, H., Walter, J., Capell, A., Steiner, H., and Haass, C. (2000) A loss of function mutant of the presenilin homologue SEL-12 undergoes aberrant endoproteolysis in *Caenorhabditis elegans* and increases abeta 42 generation in human cells, *J. Biol. Chem. 275*, 40925−40932.
25. Steiner, H., Romig, H., Pesold, B., Philipp, U., Baader, M., Citron, M., Loetscher, H., Jacobsen, H., and Haass, C. (1999) Amyloidogenic function of the Alzheimer's disease-associated presenilin 1 in the absence of endoproteolysis, *Biochemistry 38*, 14600−14605.
26. Damke, H., Baba, T., Warnock, D. E., and Schmid, S. L. (1994) Induction of mutant dynamin specifically blocks endocytic coated vesicle formation, *J. Cell Biol. 127*, 915−934.
27. Mizutani, T., Taniguchi, Y., Aoki, T., Hashimoto, N., and Honjo, T. (2001) Conservation of the biochemical mechanisms of signal transduction among mammalian Notch family members, *Proc. Natl. Acad. Sci. U.S.A. 98*, 9026−9031.
28. Pinnix, I., Musunuru, U., Tun, H., Sridharan, A., Golde, T., Eckman, C., Ziani-Cherif, C., Onstead, L., and Sambamurti, K. (2001) A novel gamma-secretase assay based on detection of the putative C-terminal fragment-gamma of amyloid beta protein precursor, *J. Biol. Chem. 276*, 481−487.
29. McLendon, C., Xin, T., Ziani-Cherif, C., Murphy, M. P., Findlay, K. A., Lewis, P. A., Pinnix, I., Sambamurti, K., Wang, R., Fauq, A., and Golde, T. E. (2000) Cell-free assays for gamma-secretase activity, *FASEB J. 14*, 2383−2386.
30. Okochi, M., Walter, J., Koyama, A., Nakajo, S., Baba, M., Iwatsubo, T., Meijer, L., Kahle, P. J., and Haass, C. (2000) Constitutive phosphorylation of the Parkinson's disease associated alpha-synuclein, *J. Biol. Chem. 275*, 390−397.
31. Chyung, J. H., and Selkoe, D. J. (2003) Inhibition of receptor-mediated endocytosis demonstrates generation of amyloid beta-protein at the cell surface, *J. Biol. Chem. 278*, 51035−51043.
32. Wolfe, M. S., Xia, W., Ostaszewski, B. L., Diehl, T. S., Kimberly, W. T., and Selkoe, D. J. (1999) Two transmembrane aspartates in presenilin-1 required for presenilin endoproteolysis and gamma-secretase activity, *Nature 398*, 513−517.
33. Kimberly, W. T., and Wolfe, M. S. (2003) Identity and function of gamma-secretase, *J. Neurosci. Res. 74*, 353−360.
34. Stevens, T. H., and Forgac, M. (1997) Structure, function and regulation of the vacuolar (H+)-ATPase, *Annu. Rev. Cell Dev. Biol. 13*, 779−808.
35. Zhao, G., Mao, G., Tan, J., Dong, Y., Cui, M. Z., Kim, S. H., and Xu, X. (2004) Identification of a new presenilin-dependent zeta-cleavage site within the transmembrane domain of amyloid precursor protein, *J. Biol. Chem. 279*, 50647−50650.
36. Qi-Takahara, Y., Morishima-Kawashima, M., Tanimura, Y., Dolios, G., Hirotani, N., Horikoshi, Y., Kametani, F., Maeda, M., Saido, T. C., Wang, R., and Ihara, Y. (2005) Longer forms of amyloid beta protein: implications for the mechanism of intramembrane cleavage by gamma-secretase, *J. Neurosci. 25*, 436−445.
37. Zhao, G., Cui, M. Z., Mao, G., Dong, Y., Tan, J., Sun, L., and Xu, X. (2005) gamma-Cleavage is dependent on zeta-cleavage during the proteolytic processing of amyloid precursor protein within its transmembrane domain, *J. Biol. Chem. 280*, 37689−37697.

BI052412W

THE JOURNAL OF BIOLOGICAL CHEMISTRY VOL. 281, NO. 8, pp. 5037–5041, February 24, 2006

Formation of Tau Inclusions in Knock-in Mice with Familial Alzheimer Disease (FAD) Mutation of Presenilin 1 (PS1)*

Received for publication, August 19, 2005, and in revised form, December 21, 2005 Published, JBC Papers in Press, December 23, 2005, DOI 10.1074/jbc.M509145200

Kentaro Tanemura[‡], Du-Hua Chui[‡1], Tetsuya Fukuda[‡], Miyuki Murayama[‡], Jung-Mi Park[‡], Takumi Akagi[§], Yoshitaka Tatebayashi[‡], Tomohiro Miyasaka[‡], Tetsuya Kimura[‡], Tsutomu Hashikawa[§], Yuka Nakano[¶], Takashi Kudo[¶], Masatoshi Takeda[¶], and Akihiko Takashima[‡2]

From the [‡]Laboratory for Alzheimer Disease and [§]Neural Architecture, Brain Science Institute, RIKEN, Wako, Saitama 351-0198, Japan and the [¶]Department of Psychiatry and Behavioral Science and Environmental Medicine, Osaka University Graduate School of Medicine, 2-2 Yamadaoka, Suita, Osaka 565-0871, Japan

Mutations in the presenilin 1 (*PS1*) gene are responsible for the early onset of familial Alzheimer disease (FAD). Accumulating evidence shows that PS1 is involved in γ-secretase activity and that FAD-associated mutations of PS1 commonly accelerate $A\beta_{1-42}$ production, which causes Alzheimer disease (AD). Recent studies suggest, however, that PS1 is involved not only in Aβ production but also in other processes that lead to neurodegeneration. To better understand the causes of neurodegeneration linked to the PS1 mutation, we analyzed the development of tau pathology, another key feature of AD, in PS1 knock-in mice. Hippocampal samples taken from FAD mutant (I213T) PS1 knock-in mice contained hyperphosphorylated tau that reacted with various phosphodependent tau antibodies and with Alz50, which recognizes the conformational change of PHF tau. Some neurons exhibited Congo red birefringence and Thioflavin T reactivity, both of which are histological criteria for neurofibrillary tangles (NFTs). Biochemical analysis of the samples revealed SDS-insoluble tau, which under electron microscopy examination, resembled tau fibrils. These results indicate that our mutant PS1 knock-in mice exhibited NFT-like tau pathology in the absence of Aβ deposition, suggesting that PS1 mutations contribute to the onset of AD not only by enhancing $A\beta_{1-42}$ production but by also accelerating the formation and accumulation of filamentous tau.

Alzheimer disease (AD)[3] is characterized pathologically by neurofibrillary tangles (NFTs), which are composed of highly phosphorylated tau, and by neuronal loss and Aβ deposition. AD is manifested symptomatically by dementia. Presenilin 1 (*PS1*), a gene identified to be responsible, in part, for early onset familial Alzheimer disease (FAD), has been cloned (1, 2). To date more than 70 mutations of the *PS1* gene have been reported (3, 4). In each mutation, early onset of AD develops with 100% penetration (3, 4). PS1 is required for γ-secretase to cleave amyloid precursor protein into Aβ species such as $A\beta_{1-40}$ and $A\beta_{1-42}$. Improper cleavage of amyloid precursor protein because of a PS1 mutation increases the production of $A\beta_{1-42}$ (5–7), a highly aggregative, neurotoxic species of Aβ that is longer than the less toxic $A\beta_{1-40}$. One hypothesis for the neurodegeneration observed in AD, therefore, is that PS1 mutation leads to increasing amounts of extracellular, neurotoxic $A\beta_{1-42}$, thereby inducing neurodegeneration (8–11).

Accumulating data suggest that, in addition to its role in $A\beta_{1-42}$ production, PS1 mutation also contributes to NFT formation. For example, PS1 conditional knock-out mice display phosphorylated tau, synaptic dysfunction, and memory impairment, even in the absence of Aβ production and deposition (12). In a related line of research, some patients clinically diagnosed with fronto-temporal dementia (FTD) have been shown to harbor PS1 mutations (13–16). Interestingly, FTD is characterized by the appearance of NFTs without Aβ deposition (17). A patient harboring the G183V PS1 mutation displayed the clinical manifestations of FTD and exhibited phospho-tau-positive Pick body pathology throughout the cortex and limbic region, without Aβ deposition. Other reports have also shown that PS1 mutations accelerate NFT formation and neuronal loss without affecting the rate of Aβ deposition (18). Thus, these data lead to the hypothesis that PS1 mutations might contribute to NFT formation as well as increase $A\beta_{1-42}$ production in FAD.

To investigate this hypothesis, we examined tau pathology in mutant PS1 I213T knock-in mice (19). This line of mice was generated with a targeted insertion of the I213T missense mutation into exon 7 of the mouse *PS1* gene using homologous recombination. Therefore, these PS1 mutant knock-in mice harbor the FAD mutation in the mouse *PS1* gene and produce PS1 I213T. Heterozygote mutant PS1 I213T mice showed no change in $A\beta_{1-40}$ levels but had increased levels of $A\beta_{1-42}$, a 1.3-fold increase when compared with wild-type mice. This $A\beta_{1-42}$ increase is comparable to that observed in human cases. Because this mouse strain shares the same PS1 genotype and related pathology as that of patients harboring the PS1 mutation, we initially expected these mice to develop the AD phenotype. The increase in murine $A\beta_{1-42}$, however, failed to lead to a corresponding Aβ deposition, possibly because murine Aβ has a different amino acid sequence that reduces its tendency to aggregate. Using this dissociation to our advantage, we investigated the Aβ deposition-independent effects of the PS1 mutation in this mouse model. We found that GSK-3β activation was followed by the accumulation of hyperphosphorylated tau in the hippocampal region, which fulfills the histological criteria for the presence of NFTs.

EXPERIMENTAL PROCEDURES

Animals—Mutant PS1 I213T knock-in mice (mPS1 mice) were maintained at the RIKEN BSI animal facilities according to the Institute guidelines for the treatment of experimental animals.

* This work was supported in part by a grant from the Ministry of Education, Science, Sports, and Culture of Japan. The costs of publication of this article were defrayed in part by the payment of page charges. This article must therefore be hereby marked "*advertisement*" in accordance with 18 U.S.C. Section 1734 solely to indicate this fact.

[1] Present address: Neuroscience Research Institute, Peking University, 38 Xue Yuan Rd., Beijing 100083, China.

[2] To whom correspondence should be addressed: Laboratory for Alzheimer Disease, RIKEN Brain Science Institute, 2-1 Hirosawa, Wako-shi, Saitama 351-0198, Japan. Tel.: 81-48-467-9632; Fax: 81-48-467-5916; E-mail: kenneth@brain.riken.jp.

[3] The abbreviations used are: AD, Alzheimer disease; PS1, presenilin 1; FAD, familial Alzheimer disease; Aβ, amyloid β protein; NFT, neurofibrillary tangles; FTD, fronto-temporal dementia; GSK-3β, glycogen synthase kinase-3β; PHFs, paired helical filaments; TBS, Tris-buffered saline; CDK5, cyclin-dependent kinase 5; JNK, c-Jun N-terminal kinase; MAP, mitogen-activated protein; TUNEL, terminal deoxynucleotidyltransferase-mediated dUTP nick end-labeling; RIPA, radioimmune precipitation assay buffer.

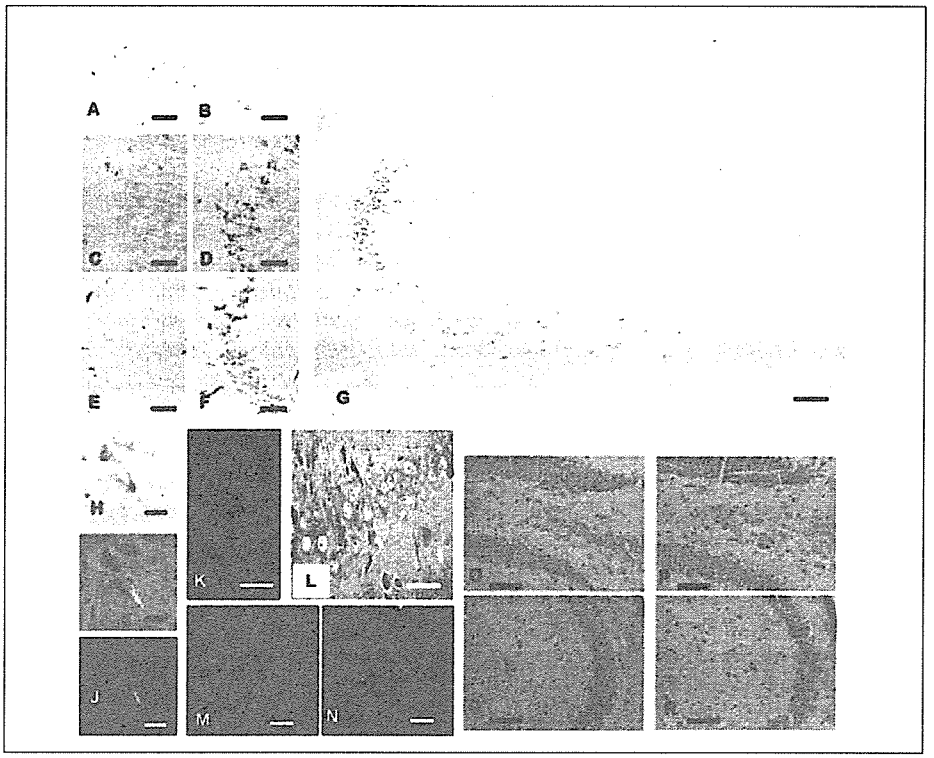

FIGURE 1. **Histochemical and histopathological assessment of brain sections from wild-type (wPS1) and mutant PS1 knock-in (mPS1) mice.** *A–G*, anti-tau immunoreactivity in hippocampal CA3 of wPS1 mice (*A, C, E*) and heterozygous mPS1 mice (*B, D, F*) at 7 months (*A, B*) and 15 months (*C–G*) of age. *A–D*, PS199 immunoreactivity; *E–G*, Alz50 immunoreactivity. The low power micrograph in *G* shows how hippocampal immunoreactivity is confined largely to CA3. *H–L*, histopathology in CA3 of heterozygous mPS1 mice at 15 months of age. *H–J*, Congo red staining without (*H*) or with (*I, J*) polarizing filters; *K*, Thioflavin T; and *L*, Gallyas silver-staining. *M* and *N*, immunoreactivity in CA3 of wPS1 (*M*) and heterozygous mPS1 mice (*N*) at 16 months of age. *M* and *N*, double immunolabeling with α-tubulin (*red*) and PS199 (*green*) antibodies. *O*, TUNEL staining of dentate gyrus in the wPS1 mouse; *P*, TUNEL staining of dentate gyrus in the homozygous mPS1 mouse; *Q*, TUNEL staining of CA3 in the wPS1 mouse; *R*, TUNEL staining of CA3 in the homozygous mPS1 mouse. Scale bars: 50 μm in *A–F* and *O–R*; 100 μm in *G*; 10 μm in *H–L*; 25 μm in *M* and *N*.

Antibodies—The following antibodies were used: mouse monoclonal anti-tubulin (DM1A, Sigma); anti-ubiquitin (Santa Cruz Biotechnology); anti-GSK3β (Transduction Laboratory); anti-MAP2 (HM2, Sigma); anti-tau Alz50, which recognizes the conformational epitope of paired helical filaments (PHFs), component of NFT (a generous gift from Dr. P. Davies, Albert Einstein College of Medicine, Bronx, NY); anti-phosphorylated tau AT8 (Innogenetics Zwijndrecht); anti-dephosphorylated tau, Tau-1 (Chemicon); rabbit polyclonal anti-tau JM (20); anti-phosphorylated tau PS199, PS262, PS396, PS404, and PS422 (BIOSOURCE), which recognize tau phosphorylated at the indicated sites; and anti-GSK3β Ser-9 (Cell Signaling).

Western Blot Analysis—Brains were homogenized in modified radioimmunoprecipitation assay (RIPA) buffer (50 mM Tris, 150 mM NaCl, 1% Nonidet P-40, 5 mM EDTA, 0.5% sodium deoxycholate, and 0.1% SDS, pH 8.0), and the suspension was centrifuged at 100,000 × *g* for 20 min at 4 °C in an Optima TL ultracentrifuge (Beckman). The pellet was washed five times with 1% SDS-Tris-buffered saline (TBS) (50 mM Tris, 150 mM NaCl, and 1% SDS, pH 8.0) followed each time by centrifugation. The SDS-insoluble pellet was solubilized in 70% formic acid, lyophilized, reconstituted in Laemmli SDS-PAGE sample buffer, and subjected to SDS-PAGE. Separated proteins were blotted onto Immobilon-P membranes (Millipore). The membranes were incubated with primary antibody then with the species-appropriate horseradish peroxidase-conjugated secondary antibody. Immunoreactivity was visualized with a chemiluminescent detection system (ECL, Amersham Biosciences). Quantitation and visual analysis of immunoreactivity were performed with a computer-linked LAS-1000 Bio-Imaging Analyzer System (Fujifilm) using the software program Image Gauge 3.0 (Fujifilm).

Glycogen Synthase Kinase (GSK)-3β Activity—Brains were homogenized in TBS (pH 7.4) and centrifuged at 100,000 × *g* for 20 min at 4 °C in an Optima TL ultracentrifuge (Beckman). Protein concentration in the supernatant was determined with a Bradford protein assay, and 10-μg samples were assayed for GSK-3β activity with an immunoprecipitation assay (21).

Ultrastructural Studies—For electron microscopy studies, SDS-insoluble materials were prepared from the brains of mPS1 mice as described above in the Western blot analysis section. The materials were mildly sonicated and dispersed in phosphate-buffered saline. The dispersed solution was absorbed onto glow-discharged supporting membranes on 400-mesh grids and prefixed by floating the grids on drops of 4% paraformaldehyde in 0.1 M phosphate buffer for 5 min. After washing, the grids were incubated with primary antibody (JM, anti-tau antibody), followed with a 5-nm colloidal gold-conjugated secondary antibody. The grids were then negatively stained with 2% sodium phosphotungstic acid, dried, and observed with a LEO 912AB electron microscope at 100 kV.

Immunohistochemical and Histopathological Studies—Brains were immersion-fixed in 10%-buffered formalin, and paraffin-embedded sections (4 μm) were prepared. PS199, Alz50, anti-MAP2, and AT8 were used as primary antibodies. After reacting the sections with species-appropriate secondary antibodies, we visualized for light microscopy analyses immunoreactive elements by treating the sections with ABC followed by DAB using Peroxidase Stain DAB kits (Nacalai Tesque Japan). PS199 and anti-α-tubulin were used as primary antibodies for confocal laser microscopy analyses. Immunoreactive elements were visualized with Alexa568-conjugated anti-mouse IgG and Alexa488-conjugated anti-rabbit IgG, and then examined with a Radiance 2000 KR3 confocal microscope (Bio-Rad). We stained some sections with Congo red and Thioflavin T, which recognize the β-sheet structure of tau fibrils, and then examined them with a light microscope equipped with crossed polarizing filters (Nikon). NFTs were identified using a standard Gallyas silver-impregnation method, which is used to assess structural changes of the brain in AD (22).

RESULTS

The Aβ levels in the brains of mPS1 knock-in mice were quantified by sandwich enzyme-linked immunoassay (23) and Western blot analysis. Similar to a previous report (19), the level of $A\beta_{1-42}$ was elevated in the brains of mPS1 mice compared with that in the brains of wild-type mice (wPS1 mice). Most of the $A\beta_{1-40}$ and $A\beta_{1-42}$ was recovered in the Triton X-100-soluble fraction, and very little was recovered in the 1% SDS-insoluble fraction, suggesting that neither $A\beta_{1-40}$ nor $A\beta_{1-42}$ aggregated and deposited within the brains of the mPS1 mice. Moreover, Aβ immunostaining in tissue sections was absent, suggesting again that neither extracellular nor intracellular Aβ accumulated *in vivo* (data not shown). Thus, murine Aβ failed to deposit in the brains of mPS1 mice, even though $A\beta_{1-42}$ levels in these brains increased.

Characterization of NFT-like Pathology in Mutant PS1 Mice—Five-month-old heterozygous mPS1 mice exhibited no pathological changes (Fig. 1*A*); however, in 7-month-old or older mice, we detected phospho-tau accumulation (PS199) in neurons in the hippocampal region (Fig. 1*B*). The prevalence and distribution of these PS199-positive neurons gradually increased and widened, respectively, with age, and in 14–16-month-old mice, we observed phospho-tau immunoreactivity in hippocampal CA3 neurons (Fig. 1*D*). By contrast, wPS1 mice did not show this pattern of phospho-tau immunoreactivity (Fig. 1, *C* and *D*). Alz50, an antibody that recognizes the conformational change of tau in PHF-tau, also labeled CA3 neurons (Fig. 1, *E–G*). In summary, these findings indicate that heterozygous mPS1 mice, whose alleles most precisely reflect the genotype of humans bearing this mutation, exhibited phospho-tau accumulation with PHF-tau epitopes, whereas wPS1 mice of the same age showed no sign of tau accumulation.

Data related to the other histological criteria for NFTs confirmed these findings. In heterozygous mPS1 mice, we observed Congo red birefringence (Fig. 1, *H–J*) and Thioflavin T reactivity (Fig. 1*K*) in hippocampal neurons. The Gallyas silver staining method revealed argyrophillic neurons in the hippocampus of mPS1 mice (Fig. 1*L*). Argyrophillic and Congo red-positive neurons were less numerous than phospho-tau-positive neurons (less than 5% of phospho-tau-positive neurons). The tau-accumulating neurons of these mice also exhibited reduced α-tubulin immunoreactivity (Fig. 1, *M* and *N*) similar to that displayed by NFT-bearing neurons. As we previously showed in tau Tg mice (24, 25), weaker α-tubulin immunoreactivity might indicate destruction of microtubules in tau-accumulating neurons in the mPS1 mice. TUNEL staining, however, revealed no signs of apoptosis in these neurons (Fig. 1, *O–R*). Taken together, these results suggest that mPS1 affects the cytoskeleton of hippocampal neurons and induces NFT-like accumulation of hyperphosphorylated tau.

Biochemical and Ultrastructural Analysis of Tau in Mutant PS1 Mice—We confirmed the accumulation of NFT-like tau in mPS1 mice with biochemical and electron microscopy analyses. Because tau becomes detergent insoluble when aggregated, we assessed the amount of tau in the SDS-insoluble fraction derived from the brains of mPS1 mice. As shown in Fig. 2*A*, small amounts of tau were recovered in the SDS-insoluble fraction from 2-month-old mPS1 mice. The amount of tau recovered in the SDS-insoluble fraction increased with aging, and a large amount of tau was recovered from 14-month-old heterozygous mPS1 mice compared with age-matched wPS1 mice. (The amount of SDS-insoluble tau in mPS1 mice was ~2% of the total tau in these mice).

We also investigated the amount of SDS-insoluble tau in different brain regions of mPS1 mice. Tau was recovered from the hippocampus, and small amounts were recovered from the cerebral cortex, striatum, and cerebellum. This might be explained by the inverse correlation of NFT with pin1 expression (26).

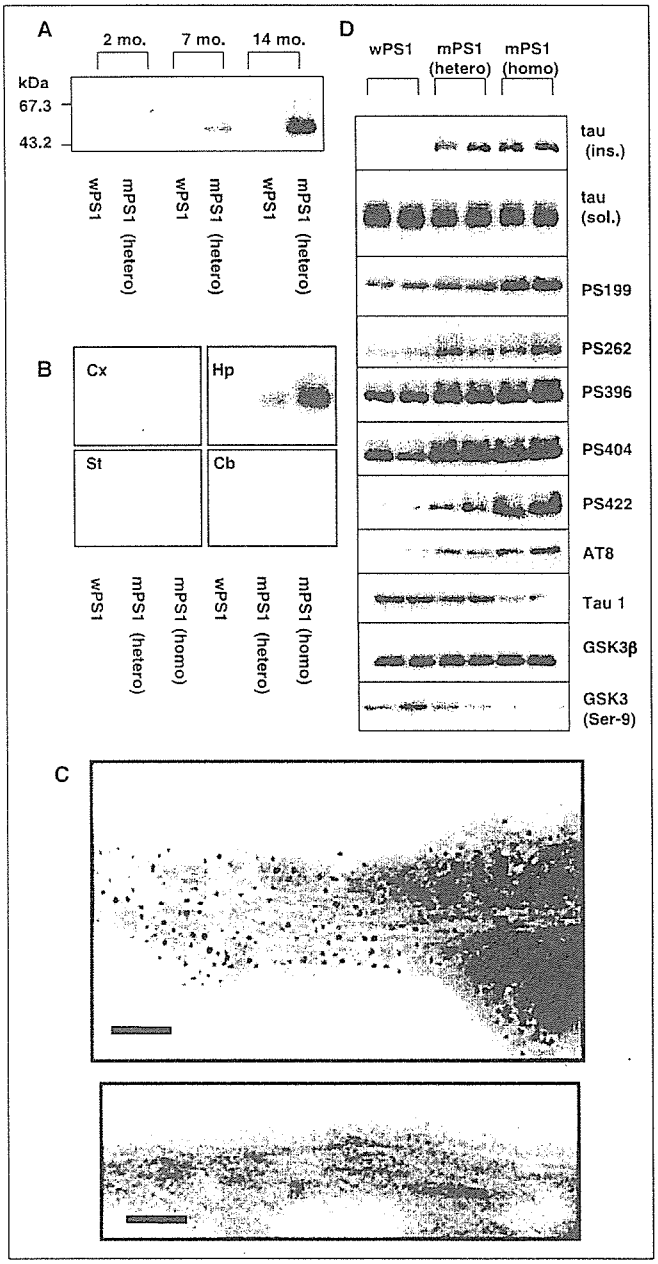

FIGURE 2. **Biochemical and electron microscopy (EM) analyses of mPS1 mice.** *A*, SDS-insoluble tau from the brains of 2-, 7-, and 14-month-old heterozygous mPS1 mice. *B*, SDS-insoluble tau in micro-dissected cortex (*Cx*), hippocampus (*Hp*), brainstem (*St*), and cerebellum (*Cb*) of 12-month-old wild-type PS1, heterozygous mPS1, and homozygous mPS1 mice. *C*, immuno-EM analysis of SDS-insoluble materials from 12-month-old heterozygous mPS1 mice. Fibrils labeled with 5-nm gold particles indicate immunoreactivity to the phosphorylation-independent tau antibody, JM (*upper panel*). Immunogold labeling was not observed on fibrils (*control*) stained in the absence of primary antibody (*lower panel*). Scale bars: 100 nm. *D*, Western blots containing SDS-insoluble and RIPA-soluble materials from the hippocampi of 14-month-old w wPS1, heterozygous mPS1, and homozygous mPS1 mice. (Lane pairs correspond to a set of two mice per mouse strain.) Order of blots (from *top* to *bottom*): SDS-insoluble tau (*tau (ins.)*; RIPA-soluble tau (*tau (sol.)*; RIPA-soluble phosphorylated tau (*PS199*, *PS262*, *PS396*, *PS404*, *PS422*, and *AT8*); unphosphorylated tau (*Tau1*), active GSK3β (*GSK3β*); and inactive GSK3β (*GSK3β (Ser-9)*).

The SDS-insoluble material recovered from mPS1 mice were further investigated with electron microscopy. As shown in Fig. 2*C*, tau-positive fibrils were detected in the SDS-insoluble fraction. These fibrils appeared to be straight tubules, about 10 nm in diameter. The biochem-

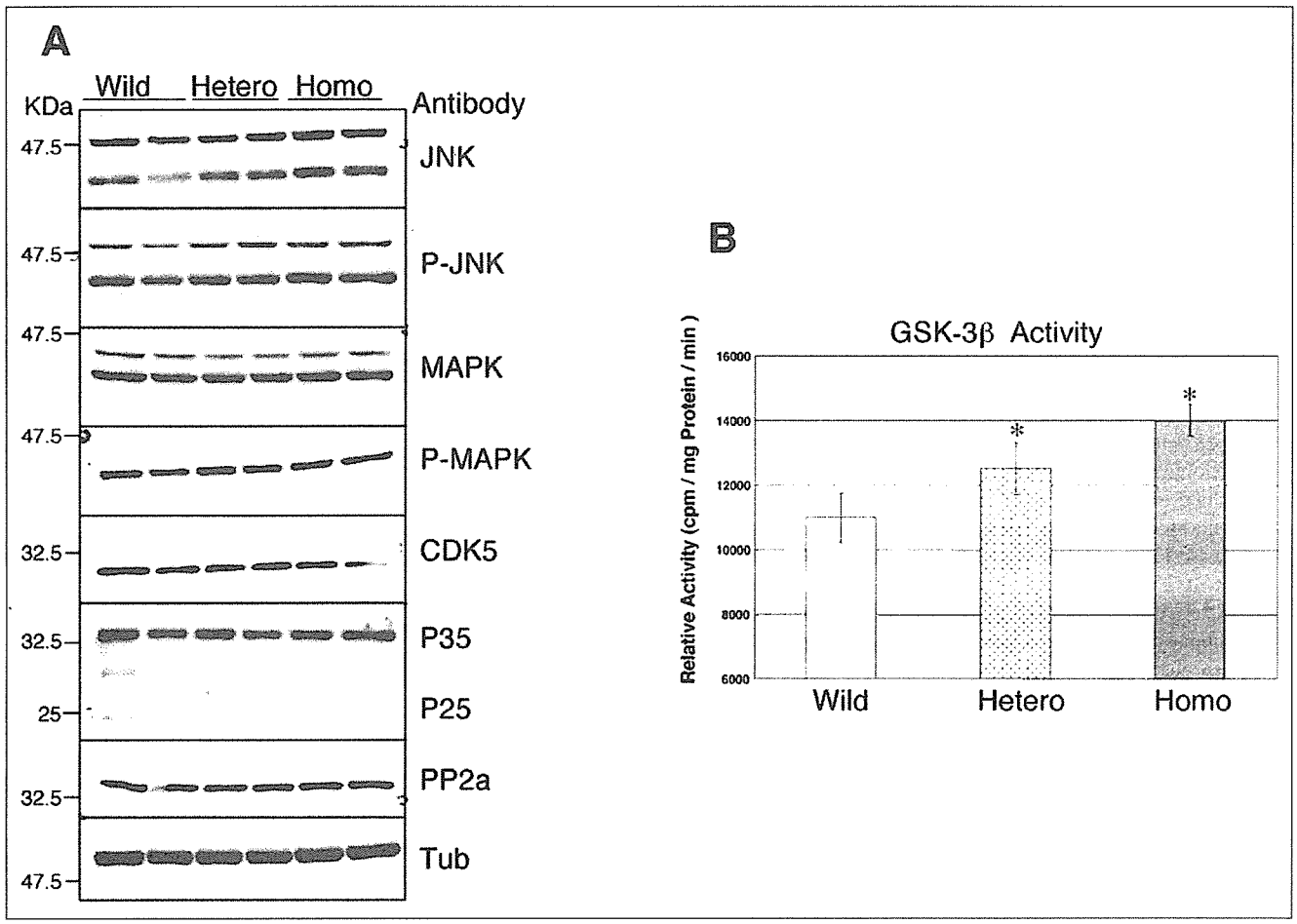

FIGURE 3. **Tau kinase activity in 12-month-old mPS1 mice.** *A*, hippocampal lysates from wPS1, heterozygous mPS1, and homozygous mPS1 mice were analyzed with Western blotting and antibodies against tau kinases and phosphatases: total JNK (*JNK*); phospho-JNK (*P-JNK*); MAP kinase (*MAPK*); phosphorylated MAP kinase (*PMAPK*); CDK5; the CDK5 activators, p35 and p25; and phosphatase 2a (*PP2a*)). A blot stained with anti-tubulin antibody (*Tub*) represents the control. *B*, GSK-3β activity in immunoprecipitated brain samples derived from wPS1, heterozygous mPS1, and homozygous mPS1 mice were determined with an assay that measures the incorporation of ^{32}P into a GSK-3β substrate peptide. Data are expressed as averages ± S.D. (*, $p < 0.05$; $n = 3$).

ical and ultrastructural analyses strongly suggest that NFT-like tau aggregation formed primarily in hippocampal neurons of mPS1 mice.

The NFTs found in AD brains contain highly phosphorylated tau (27). Hyperphosphorylation of tau leads to the formation of fibrillar tau (28). To determine whether tau hyperphosphorylation also occurs in mPS1 mice, we examined the extent of tau phosphorylation in 14-month-old wPS1, heterozygous mPS1, and homozygous mPS1 mice (Fig. 2*D*). Immunoblotting with various phosphorylation-dependent anti-tau antibodies revealed that the amount of SDS-insoluble tau was nearly the same in heterozygous and homozygous mPS1 mice (Fig. 2*D*, *tau(ins.)*). This amount, however, was greater than that in wPS1 mice. Although the total amounts of tau in soluble fractions from the three types of mice were similar (*i.e.* bands had slower mobility than the unphosphorylated Tau-1-immunoreactive band) (Fig. 2*D*, *tau(sol.)*), the amounts of phosphorylated tau immunostained by PS199, PS262, PS396, PS404, PS422, and AT8 were elevated in the heterozygous and homozygous mPS1 mice compared with those in the wPS1 mice. The extent of tau phosphorylation at the AT8, PS422, and PS199 epitopes appeared to depend on the number of mPS1 alleles present in the mice, as shown by the comparatively greater immunosignal intensity of samples derived from homozygous than in heterozygous mPS1 mice, suggesting that mPS1 expression affects the hyperphosphorylation of tau. The immunostaining intensity of Tau-1, an antibody that recognizes unphosphorylated tau, also correlated with genotype. Tau-1 immunoreactivity was greater in samples derived from wPS1 mice than in heterozygous and homozygous mPS1 mice (wPS1 > heterozygous mPS1 > homozygous mPS1), confirming that mPS1 induced the hyperphosphorylation of tau.

GSK-3β, Tau Kinase, and Tau Phosphatase Activity—Activation of GSK-3β, a known tau kinase, was also associated with mPS1 genotype. Although total GSK-3β levels were similar among wPS1, heterozygous mPS1, and homozygous mPS1 mice, inactive GSK-3β (GSK-3β phosphorylated at Ser-9) levels varied inversely with the number of mPS1 alleles present (Fig. 2*D*; GSK3β and GSK3β(*Ser-9*)). This inverse correlation was confirmed by comparing the GSK-3β activity in immunoprecipitated brain samples derived from wPS1, heterozygous mPS1, and homozygous mPS1 mice (Fig. 3*B*). This assay revealed elevated GSK-3β activity in heterozygous mPS1 compared with wPS1 mice ($p < 0.05$; $n = 3$), and also in homozygous mPS1 mice compared with heterozygous mice ($p < 0.05$; $n = 3$). Taken together, we conclude that the mutant PS1 activated GSK-3β, thereby enhancing tau phosphorylation and resulting in the formation of NFT-like tau aggregates (Figs. 1 and 2). These results support those from a previous report (20).

We also investigated how other kinases and phosphatases may contribute to tau phosphorylation in mPS1 mice. As shown in Fig. 3*A*, levels of the active forms of phosphorylated JNK; phosphorylated MAP kinase; CDK5;

the CDK5 activators p35 and p25; and PP2a were similar among wPS1, heterozygous mPS1, and homozygous mPS1 mice, indicating that the tau phosphorylation mediated by these enzymes are not affected by the PS1 mutation. Nonetheless, other mechanisms are expected to be involved in the mPS1-induced hyperphosphorylation of tau, because GSK-3β alone cannot phosphorylate all of the phosphorylation sites in tau.

DISCUSSION

In the present study, we demonstrated that the brains of mice harboring a PS1 mutation accumulated NFT-like phospho-tau. Biochemical analysis of SDS-insoluble tau revealed tau fibrils. These NFT-like tau inclusions were similar to those observed in FTDP-17 mutant tau transgenic mice (24, 25, 28), in mice overexpressing p25, a CDK5 activator (29), and in Pin1 knock-out mice (26). The neurons of other PS1 knock-in and mutant PS1 transgenic mice; however, failed to show cytoskeletal changes (30, 31). To create their mutant PS1 knock-in mice, Guo *et al.* (32) used a hybrid mouse composed of 129SV and C57BL6 strains, whereas in the present study we used mice resulting from 10 generations of crossbreeding with C57BL6J mice. The genetic background of our mice, which is most likely to be different from the backgrounds of mice used in previously studies, could have influenced how the PS1 mutation contributed to NFT formation and cytoskeletal changes. Another possible explanation for the apparent discrepancy between our findings and others is that our PS1 knock-in mice harbored a different PS1 mutation from that harbored by mutant PS1 knock-in mice developed by other laboratories.

Previously, we found certain PS1 mutations that increase $A\beta_{1-42}$ levels are poor predictors for the onset of FAD (5). Our present results, however, suggest that the accumulation of NFT-like tau could determine the onset of AD. These two differing outcomes would also explain why some PS1 mutations accelerate NFT formation and neuronal loss without accelerating Aβ deposition (18). Thus, PS1 mutations that accelerate both NFT formation and $A\beta_{1-42}$ production may further accelerate related neuropathologies, suggesting that the cause of early onset AD may be related to a PS1 mutation.

The mechanism underlying the mutant PS1-associated accumulation of NFTs may involve the activation of GSK-3β. Our results indicate that GSK-3β is activated in our mPS1 knock-in mice; this is consistent with other mPS1 transgenic mice. Recently, wild-type PS1 has been shown to activate PI3 kinase/Akt signaling by promoting the association of cadherin and PI 3-kinase, whereas mutant PS1 was unable to do so (32). Thus, mutant PS1 appears to impair PI 3-kinase/Akt signaling by affecting selected signaling receptors (33) or by reducing cadherin/PI3 kinase association (32), which eventually leads to the activation of GSK-3β. Whereas the mutant PS1-associated activation of GSK-3β occurred in young mice, tau accumulation occurred only later on in older mice. This led us to hypothesize that, by some mechanism, phosphorylated tau degrades before it aggregates. This unknown mechanism is then inactivated during aging, leading to the accumulation and aggregation of tau that occurs in aged individuals.

Patients harboring the FAD mutation of PS1 develop AD with 100% penetration. Based on our results, we propose that the PS1 mutation in FAD leads to the early onset of AD through the activation of GSK-3β, which leads to NFT formation and the loss of neurons and synapses. Moreover, we believe that the rate of GSK-3β activation is accelerated by extracellular Aβ oligomers. The exact molecular mechanism mediating the mutant PS1-induced activation of GSK-3β requires clarification to further our understanding of how AD develops.

REFERENCES

1. Sherrington, R., Rogaev, E. I., Liang, Y., Rogaeva, E. A., Levesque, G., Ikeda, M., Chi, H., Lin, C., Li, G., Holman, K., Tsuda, T., Mar, L., Foncin, J.-F., Bruni, A. C., Montesi, M. P., Sorbi, S., Rainero, I., Pinessi, L., Nee, L., Chumakov, I., Pollen, D., Brookes, A., Sanseau, P., Polinsky, R. J., Wasco, W., Da Silva, H. A. R., Haines, J. L., Pericak-Vance, M. A., Tanzi, R. E., Roses, A. D., Fraser, P. E., Rommens, J. M., and St. George-Hyslop, P. H. (1995) *Nature* **375,** 754–760
2. Cruts, M., Backhovens, H., Wang, S. Y., Van Gassen, G., Theuns, J., De Jonghe, C. D., Wehnert, A., De Voecht, J., De Winter, G., and Cras, P. (1995) *Hum. Mol. Genet.* **4,** 2363–2371
3. St George-Hyslop, P. H., and Petit, A. (2005) *C. R. Biol.* **328,** 119–130
4. St George-Hyslop, P. H. (2000) *Biol. Psychiatry* **47,** 183–199
5. Murayama, O., Honda, T., Mercken, M., Murayama, M., Yasutake, K., Nihonmatsu, N., Nakazato, Y., Michel, G., Song, S., Sato, K., Takahashi, H., and Takashima, A. (1997) *Neurosci. Lett.* **229,** 61–64
6. Scheuner, D., Eckman, C., Jensen, M., Song, X., Citron, M., Suzuki, N., Bird, T. D., Hardy, J., Hutton, M., Kukull, W., Larson, E., Levy-Lahad, E., Viitanen, M., Peskind, E., Poorkaj, P., Schellenberg, G., Tanzi, R., Wasco, W., Lannfelt, L., Selkoe, D., and Younkin, S. (1996) *Nat. Med.* **2,** 864–870
7. Holcomb, L., Gordon, M. N., McGowan, E., Yu, X., Benkovic, S., Jantzen, P., Wright, K., Saad, I., Mueller, R., Morgan, D., Sanders, S., Zehr, C., O'Campo, K., Hardy, J., Prada, C. M., Eckman, C., Younkin, S., Hsiao, K., and Duff, K. (1998) *Nat. Med.* **4,** 97–100
8. Chang, P., and Su, Y. (2000) *Brain Res. Brain Res. Protoc.* **6,** 6–12
9. Klein, A. M., Kowall, N. W., and Ferrante, R. J. (1999) *Ann. N. Y. Acad. Sci.* **893,** 314–320
10. Morelli, L., Prat, M. I., and Castano, E. M. (1999) *Cell Tissue Res.* **298,** 225–232
11. Butterfield, D. A. (2002) *Free Radic. Res.* **36,** 1307–1313
12. Yu, H., Saura, C. A., Choi, S. Y., Sun, L. D., Yang, X., Handler, M., Kawarabayashi, T., Younkin, L., Fedeles, B., Wilson, M. A., Younkin, S., Kandel, E. R., Kirkwood, A., and Shen, J. (2001) *Neuron* **31,** 713–726
13. Amtul, Z., Lewis, P. A., Piper, S., Crook, R., Baker, M., Findlay, K., Singleton, A., Hogg, M., Younkin, L., Younkin, S. G., Hardy, J., Hutton, M., Boeve, B. F., Tang-Wai, D., and Golde, T. E. (2002) *Neurobiol. Dis.* **9,** 269–273
14. Dermaut, B., Kumar-Singh, S., Engelborghs, S., Theuns, J., Rademakers, R., Saerens, J., Pickut, B. A., Peeters, K., van den Broeck, M., Vennekens, K., Claes, S., Cruts, M., Cras, P., Martin, J. J., Van Broeckhoven, C., and De Deyn, P. P. (2004) *Ann. Neurol.* **55,** 617–626
15. Tang-Wai, D., Lewis, P., Boeve, B., Hutton, M., Golde, T., Baker, M., Hardy, J., Michels, V., Ivnik, R., Jack, C., and Petersen, R. (2002) *Dement. Geriatr. Cogn. Disord.* **14,** 13–21
16. Evin, G., Smith, M. J., Tziotis, A., McLean, C., Canterford, L., Sharples, R. A., Cappai, R., Weidemann, A., Beyreuther, K., Cotton, R. G., Masters, C. L., and Culvenor, J. G. (2002) *Neuroreport* **13,** 719–723
17. Yoshiyama, Y., Lee, V. M., and Trojanowski, J. Q. (2001) *Curr. Neurol. Neurosci. Rep.* **1,** 413–421
18. Gomez-Isla, T., Growdon, W. B., McNamara, M. J., Nochlin, D., Bird, T. D., Arango, J. C., Lopera, F., Kosik, K. S., Lantos, P. L., Cairns, N. J., and Hyman, B. T. (1999) *Brain* **122,** 1709–1719
19. Nakano, Y., Kondoh, G., Kudo, T., Imaizumi, K., Kato, M., Miyazaki, J. I., Tohyama, M., Takeda, J., and Takeda, M. (1999) *Eur. J. Neurosci.* **11,** 2577–2581
20. Takashima, A., Murayama, M., Murayama, O., Kohno, T., Honda, T., Yasutake, K., Nihonmatsu, N., Mercken, M., Yamaguchi, H., Sugihara, S., and Wolozin, B. (1998) *Proc. Natl. Acad. Sci. U. S. A.* **95,** 9637–9641
21. Van Lint, J., Khandelwal, R. L., Merlevede, W., and Vandenheede, J. R. (1993) *Anal. Biochem.* **208,** 132–137
22. Iqbal, K., Braak, E., Braak, H., Zaidi, T., and Grundke-Iqbal, I. (1991) *Neurobiol. Aging* **12,** 357–361
23. Sun, X., Cole, G. M., Chu, T., Xia, W., Galasko, D., Yamaguchi, H., Tanemura, K., Frautschy, S. A., and Takashima, A. (2002) *Neurobiol. Aging* **23,** 195–203
24. Tatebayashi, Y., Miyasaka, T., Chui, D. H., Akagi, T., Mishima, K., Iwasaki, K., Fujiwara, M., Tanemura, K., Murayama, M., Ishiguro, K., Planel, E., Sato, S., Hashikawa, T., and Takashima, A. (2002) *Proc. Natl. Acad. Sci. U. S. A.* **99,** 13896–13901
25. Tanemura, K., Murayama, M., Akagi, T., Hashikawa, T., Tominaga, T., Ichikawa, M., Yamaguchi, H., and Takashima, A. (2002) *J. Neurosci.* **22,** 133–141
26. Liou, Y. C., Sun, A., Ryo, A., Zhou, X. Z., Yu, Z. X., Huang, H. K., Uchida, T., Bronson, R., Bing, G., Li, X., Hunter, T., and Lu, K. P. (2003) *Nature* **424,** 556–561
27. Lee, V. M., Balin, B. J., Otvos, L., Jr., and Trojanowski, J. Q. (1991) *Science* **251,** 675–678
28. Sato, S., Tatebayashi, Y., Akagi, T., Chui, D. H., Murayama, M., Miyasaka, T., Planel, E., Tanemura, K., Sun, X., Hashikawa, T., Yoshioka, K., Ishiguro, K., and Takashima, A. (2002) *J. Biol. Chem.* **277,** 42060–42065
29. Cruz, J. C., Tseng, H. C., Goldman, J. A., Shih, H., and Tsai, L. H. (2003) *Neuron* **40,** 471–483
30. Siman, R., Reaume, A. G., Savage, M. J., Trusko, S., Lin, Y. G., Scott, R. W., and Flood, D. G. (2000) *J. Neurosci.* **20,** 8717–8726
31. Guo, Q., Sebastian, L., Sopher, B. L., Miller, M. W., Ware, C. B., Martin, G. M., and Mattson, M. P. (1999) *J. Neurochem.* **72,** 1019–1029
32. Baki, L., Shioi, J., Wen, P., Shao, Z., Schwarzman, A., Gama-Sosa, M., Neve, R., and Robakis, N. K. (2004) *EMBO J.* **23,** 2586–2596
33. Kang, D. E., Sang Yoon, I., Repetto, E., Busse, T., Yermian, N., Ie, I., and Koo, E. H. (2005) *J. Biol. Chem.* **280,** 31537–31547

Available online at www.sciencedirect.com
ScienceDirect
Biochemical and Biophysical Research Communications 351 (2006) 602–611
BBRC
www.elsevier.com/locate/ybbrc

TDP-43 is a component of ubiquitin-positive tau-negative inclusions in frontotemporal lobar degeneration and amyotrophic lateral sclerosis

Tetsuaki Arai [a,1,*], Masato Hasegawa [b,1,*], Haruhiko Akiyama [a], Kenji Ikeda [c], Takashi Nonaka [b], Hiroshi Mori [d], David Mann [e], Kuniaki Tsuchiya [f], Mari Yoshida [g], Yoshio Hashizume [g], Tatsuro Oda [h]

[a] *Department of Psychogeriatrics, Tokyo Institute of Psychiatry 2-1-8 Kamikitazawa, Setagaya-ku, Tokyo 156-8585, Japan*
[b] *Department of Molecular Neurobiology, Tokyo Institute of Psychiatry 2-1-8 Kamikitazawa, Setagaya-ku, Tokyo 156-8585, Japan*
[c] *Zikei hospital 100-2 Urayasuhonmachi, Okayama-shi, Okayama 702-8508, Japan*
[d] *Department of Neuroscience, Osaka City University School of Medicine, 1-4-3 Asahimachi, Abenoku, Osaka 545-8585, Japan*
[e] *Greater Manchester Neurosciences Centre, University of Manchester, Hope Hospital, Salford M6 8HD, UK*
[f] *Department of Laboratory Medicine and Pathology, Tokyo Metropolitan Matsuzawa Hospital, 2-1-1 Kamikitazawa, Setagaya-ku, Tokyo 156-0057, Japan*
[g] *Department of Neuropathology, Institute for Medical Science of Aging, Aichi Medical University, 21 Karimata, Yazako, Nagakute-cho, Aichi-gun, Aichi 480-1195, Japan*
[h] *Department of Neuropsychiatry, National Shimofusa Mental Hospital, Chiba 266-0007, Japan*

Received 2 October 2006
Available online 30 October 2006

Abstract

Ubiquitin-positive tau-negative neuronal cytoplasmic inclusions and dystrophic neurites are common pathological features in frontotemporal lobar degeneration (FTLD) with or without symptoms of motor neuron disease and in amyotrophic lateral sclerosis (ALS). Using biochemical and immunohistochemical analyses, we have identified a TAR DNA-binding protein of 43 kDa (TDP-43), a nuclear factor that functions in regulating transcription and alternative splicing, as a component of these structures in FTLD. Furthermore, skein-like inclusions, neuronal intranuclear inclusions, and glial inclusions in the spinal cord of ALS patients are also positive for TDP-43. Dephosphorylation treatment of the sarkosyl insoluble fraction has shown that abnormal phosphorylation takes place in accumulated TDP-43. The common occurrence of intracellular accumulations of TDP-43 supports the hypothesis that these disorders represent a clinicopathological entity of a single disease, and suggests that they can be newly classified as a proteinopathy of TDP-43.

Keywords: Phosphorylation; Accumulation; Insoluble; Neurite; Glia; Motoneuron; Spinal cord; Mass spectrometry; Immunoblot; Immunohistochemistry

Frontotemporal dementia (FTD) is a clinical term applied to progressive dementia with behavioral changes and/or language dysfunction. Pathological diagnosis of FTD can be classified into three major categories [1]. The first category consists of tauopathies including Pick's disease (PiD), corticobasal degeneration (CBD), progressive supranuclear palsy (PSP), and FTD with parkinsonism linked to chromosome 17 (FTDP-17). The second is frontotemporal lobar degeneration (FTLD) with ubiquitin-positive tau-negative neuronal cytoplasmic inclusions (NCI). This can be divided into two subtypes. One is FTLD with motor neuron disease (MND), which is also known as presenile dementia with MND [2] or amyotrophic lateral sclerosis (ALS) with dementia [3,4]. The other is FTLD with MND-type inclusions but without MND,

* Corresponding authors. Fax: +81 3 3329 8035.
E-mail addresses: arai@prit.go.jp (T. Arai), masato@prit.go.jp (M. Hasegawa).
[1] These authors contributed equally to this work.

0006-291X/$ - see front matter © 2006 Elsevier Inc. All rights reserved.
doi:10.1016/j.bbrc.2006.10.093

which is also designated as motor neuron disease-inclusion dementia (MNDID) [5] or atypical PiD without Pick bodies [6,7]. The last category is FTLD without tau- or ubiquitin-positive inclusions, also known as dementia lacking distinctive histology [8]. It has been reported that FTLD with MND-type inclusions but without MND (FTLD-MND-type) is the most common in FTD [9].

The appearance of ubiquitin-positive tau-negative NCI was first recognized in patients with ALS [10], and was subsequently found in those with FTLD with MND (FTLD-MND) [4,11] and in FTLD-MND-type [5,6,12]. The overlap of such ubiquitin pathology suggests that a common pathological process exists among these disorders [5,12–14]. To clarify this issue, it is important to identify key components of the inclusions. Thus far, p62, a ubiquitin binding protein, and a ubiquitin-like protein (neural precursor cell-expressed and developmentally down-regulated 8 (NEDD8)), have been reported to be incorporated in ubiquitin-positive inclusions in these disorders [15,16]. However, these proteins are also present in other ubiquitinated inclusions such as neurofibrillary tangles, Lewy bodies, and glial cytoplasmic inclusions [16,17], indicating that their accumulation is not a specific process for FTLD-MND-type, FTLD-MND, or ALS.

A subset of patients with familial FTLD has been reported to have ubiquitin-positive neuronal intranuclear inclusions (NII) and/or NCI similar to those in sporadic cases [18–21]. Recently, null mutations in the gene encoding progranulin (PGRN), a growth factor involved in multiple processes including development, wound repair, inflammation, and tumorigenesis, have been identified in several FTLD families with NII and NCI linked to chromosome 17 [22–25]. It is proposed that PGRN haploinsufficiency leads to neurodegeneration due to reduced PGRN-mediated neuronal survival [22,23]. Immunohistochemical examination has shown no staining of NCI and NII for PRGN, indicating that the disease does not cause accumulation of PRGN [22–24]. Familial FTD with inclusion body myopathy and Paget disease of bone is caused by mutations in the valosin-containing protein (VCP) gene, a member of AAA-ATPase gene super family [26]. It has been reported that these families have ubiquitin-positive NII and dystrophic neurites but rare NCI, and most of the ubiquitin-positive structures are negative for VCP [21]. Thus, the major component of the ubiquitinated proteins in NCI and NII still remains unknown.

In the present study, using biochemical and immunohistochemical analyses, we have identified TAR DNA-binding protein of 43 kDa (TDP-43), a nuclear protein which is involved in transcriptional repression and alternative splicing [27,28], as a component of ubiquitin-positive tau-negative inclusions in FTLD-MND-type, FTLD-MND, and ALS. These results support the notion that these disorders represent a clinicopathological spectrum of a single disease. The results of biochemical analysis suggest that abnormal phosphorylation of TDP-43 may be involved in the pathogenesis of these disorders.

Materials and methods

Materials. Brains from six cases of FTLD-MND-type, 3 with FTLD-MND, 4 with ALS, 5 with Alzheimer's disease (AD), 7 with PiD with Pick bodies, 3 with dementia with Lewy bodies (DLB), 3 with multiple system atrophy (MSA), one each case of CBD, PSP, and tangle only dementia, and six controls without neurological symptoms were employed in this study. The age, sex, brain weight, brain regions examined, and diagnosis are given in Table 1.

Table 1
Description of the subjects

Case No.	Age (years)	Sex	BW (g)	Region	Clinical diagnosis
1	67	M	1250	Hip, T	FTLD-MND-type
2	59	M	na	Hip, T	FTLD-MND-type
3	68	M	1210	F	FTLD-MND-type
4	69	M	1166	F	FTLD-MND-type
5	68	F	1120	Hip, T	FTLD-MND-type
6	81	M	950	Hip, T	FTLD-MND-type
7	49	F	1115	T	FTLD-MND
8	65	F	na	T	FTLD-MND
9	72	F	1070	SC (L)	FTLD-MND
10	69	F	na	Caudate	ALS
11	55	M	1650	SC (L, S)	ALS
12	72	F	1330	SC (L, S)	ALS
13	48	M	1400	SC (L, S)	ALS
14	84	F	960	T	AD
15	68	F	1040	T	AD
16	75	M	1000	T	AD
17	89	M	1310	Hip, T	AD
18	83	F	940	Hip, T	AD
19	67	F	na	Hip, T	PiD
20	51	F	530	Hip, T	PiD
21	76	M	na	Hip, T	PiD/AD
22	71	M	680	F	PiD
23	75	M	1080	F	PiD
24	56	F	950	Hip, T	PiD
25	67	F	1120	Hip, T	PiD
26	67	M	840	Poc/Prec	CBD
27	72	M	1290	Poc/Prec	PSP
28	86	F	945	Hip	Tangle only dementia
29	82	F	1050	Hip, T, SN	DLB
30	85	F	1040	T	DLB
31	51	M	1050	T	DLB
32	70	M	na	P	MSA
33	49	M	1450	P	MSA
34	56	F	1130	SN	MSA
35	75	M	1280	SC (L)	Sch, pneumonia
36	56	M	1150	Hip, T	Sch, lung cancer
37	70	F	1220	Hip, T	Gastric cancer
38	72	M	1300	Hip, T	Sch, pneumonia
39	81	F	1110	Hip, T	Retroperitoneal tumor
40	65	M	1270	Hip, T	Dilated cardiomyopathy

BW, brain weight; Hip, hippocampus; T, temporal; F, frontal; SC, spinal cord; L, lumbar; Poc/Prec, postcentral/precentral; SN, substantia nigra; FTLD, frontotemporal lobar degeneration; MND, motor neuron disease; ALS, amyotrophic lateral sclerosis; AD, Alzheimer's disease; PiD, Pick's disease; CBD, corticobasal degeneration; PSP, progressive supranuclear palsy; DLB, dementia with Lewy bodies; MSA, multiple system atrophy; Sch, schizophrenia; na, not available.

Fractionation of brain extracts. Frozen temporal or frontal cortex (0.5 g) from 4 cases of FTLD-MND-type (cases 1–4) and a case of FTLD-MND (case 7), 3 with AD (cases 14–16), 2 with PiD (cases 22, 23), 2 with DLB (cases 29, 30), 2 with MSA (cases 32, 33), and a control (case 37) were homogenized in 10 volumes (5 ml) of buffer A (10 mM Tris–HCl, pH 7.5, 1 mM EGTA, 10% sucrose, and 0.8 M NaCl). After addition of another 5 ml of buffer A containing 2% Triton X-100, the homogenate was incubated for 30 min at 37 °C and spun at 100,000*g* for 30 min at 4 °C. The resultant pellet was homogenized in 5 volumes of buffer A, followed by an incubation for 30 min at 37 °C with 1% sarkosyl. The homogenate was then spun at 100,000*g* for 30 min at room temperature. The sarkosyl-insoluble pellet was homogenized in 4 volumes of buffer A containing 1% CHAPS and spun at 100,000*g* for 20 min at room temperature. The pellet was sonicated in 0.2 volumes of 7 M guanidine hydrochloride, followed by overnight dialysis at 4 °C against 30 mM Tris–HCl (pH 7.5).

For dephosphorylation, the sample was incubated with Lambda protein phosphatase (1600 U/ml; New England Biolabs, Ipswich, MA) for 30 min at 30 °C according to manufacturer's instruction.

In gel digestion and LC/MS/MS analysis. The dialyzed samples from FTLD-MND-type, AD, DLB, and a control were run on SDS–PAGE using 4–20% polyacrylamide gel (PAG mini, Daiichi, Tokyo). After staining with Coomassie brilliant blue R-250 (CBB), each lane was cut out every 5 mm from the bottom to the top of the running gel. The resultant all gel pieces were cut into 1 × 1 mm cubes and washed twice with 50% acetonitrile in 0.1 M ammonium carbonate and dried in a vacuum centrifuge. The gel pieces were then rehydrated in buffer containing 1 μg/ml trypsin (Promega Inc., Madison, WI) and 0.1 M ammonium carbonate, and incubated for 16 h at 37 °C. The digested peptides were extracted using 50% acetonitrile and 5% formic acid, and dried. They were dissolved in 0.1% trifluoroacetic acid, 2% acetonitrile and an aliquot was separated on a Develosil ODS-HG-5 column (0.15 × 50 mm, Nomura Chemical Company, Aichi, Japan) at a flow rate of 300 nl/min using nano-flow HPLC (Dina; TYK Tech Company) and analyzed by ion-trap spectrometry (LCQ Advantage; Thermo Electron Corporation, Waltham, MA). The MS/MS data files were searched using the Turbo Sequest algorithm within the Bioworks software (Thermo Electron, CA). Results were filtered using two independent measures for the accuracy of matches: *p* value and a cross correlation (XCorr) score.

Immunohistochemical analysis. Small blocks of brain were dissected at autopsy or from fresh frozen brain samples and fixed in 4% paraformaldehyde in 0.1 M phosphate buffer (pH 7.4) for 2 days. Following cryoprotection in 15% sucrose in 0.01 M phosphate-buffered saline (PBS) (pH 7.4), blocks were cut on a freezing microtome at 30 μm thickness. The free floating sections were immunostained with two well-characterized commercial antibodies: a polyclonal (10782-1-AP, ProteinTech Group Inc., Chicago, IL; 1:2000) and a monoclonal (2E2-D3, Abnova Corporation, Taipei, Taiwan; 1:1000) specific for TDP-43. A monoclonal antibody to ubiquitin (DF2; 1:200) [29] and a polyclonal antibody to tau (A0024, DakoCytomation, Carpinteria, CA; 1:30000) were also used. For analyzing the spinal cord from FTLD-MND and ALS cases, 10% formalin-fixed and paraffin-embedded blocks were dissected at 10 μm and immunostained using the primary antibodies with 10 times lower dilution than in floating sections.

The sections were incubated with the primary antibody for 72 h in the cold. Following treatment with the appropriate secondary antibody, labeling was detected using the avidin-biotinylated HRP complex (ABC) system coupled with a diaminobenzidine (DAB) reaction to yield a brown precipitate. In some sections, the DAB reaction was intensified with nickel ammonium sulfate to yield a dark purple precipitate. Pretreatment of tissues by autoclaving in 10 mM sodium citrate buffer for 10 min at 120 °C was needed for staining with 2E2–D3.

Immunoblot analysis. After SDS–PAGE, proteins in the gel were electrotransferred onto a polyvinylidene difluoride membrane (Millipore Corp., Bedford, MA). After blocking with 3% gelatin in Tris-buffered saline (20 mM Tris–HCl, pH 7.5, 500 mM NaCl), membranes were incubated overnight with the polyclonal and monoclonal antibodies to TDP-43, 10782-1-AP (1:2000) and 2E2–D3 (1:1000), HT7 (Innogenetics, Gent, Belgium; 1:3000) and anti-PSer129 (1:3000) [30]. Following incubation with an appropriate biotinylated secondary antibody, labeling was detected using ABC system (Vector Lab., Burlingame, CA) coupled with a DAB reaction intensified with nickel chloride.

Results

Fig. 1 illustrates the representative results of SDS–PAGE on the sarkosyl insoluble fraction from cases of FTLD-MND-type, DLB, AD, and control. Western blotting using a mixture of anti-PSer129, a phosphorylation-dependent antibody to α-synuclein, and HT7, a phosphorylation-independent antibody to tau, showed, as previously reported [30,31], an intense band of α-synuclein in DLB (A, lane 3), and a triplet of 68, 64, and 60 kDa typical for hyperphosphorylated tau (PHF-tau) in AD (A, lane 4), but virtually nothing in the control (A, lane 1). In the FTLD-MND-type case, only a small amount of the PHF-tau bands are shown (A, lane 2). This finding corresponds to the mild occurrence of neurofibrillary tangles and neuropil threads in the cerebral cortex in this case (data not shown). CBB staining of the identical gel to that blotted showed virtually no difference among cases (B).

LC/MS/MS analysis of samples obtained from the digested gel identified the sequences of α-synuclein in DLB and those of tau in AD, proving the adequacy of the method to pick up the accumulated proteins (data not shown). The proteins identified by the database search in the same molecular weight area were compared among FTLD-MND-type, AD, DLB, and the control. By analyzing the area below 40 kDa, we identified the peptide with the amino acid sequence of FGGNPGGFGNQGGFG NSR in the FTLD-MND-type case (Fig. 2). This sequence was identical with the sequence of TDP-43 (276–293; according to the report by Ou et al. [27]).

By immunohistochemistry using the antibodies to TDP-43, nuclei of neurons and glial cells were positive in the gray and whiter matters of the temporal, frontal, and parietal lobes, the hippocampus (Fig. 3A and B), the brain stem, and the cerebellum in all cases examined. In the FTLD-MND and FTLD-MND-type cases, in addition to such nuclear stainings, the antibodies recognized NCI and dystrophic neurites in the hippocampal region and temporal cortex (Fig. 3C–F). The morphology of these TDP-43 positive inclusions and neurites was comparable to that of ubiquitin-positive NCI and neurites (Fig. 3G and H). Ubiquitin-positive dystrophic neurites in the caudate nucleus were also positive for TDP-43 in a case of ALS (data not shown).

In the spinal cord of the ALS and FTLD-MND cases, skein-like inclusions were positive for ubiquitin (Fig. 4A) as previously reported [32,33]. They were also positive for both polyclonal and monoclonal antibodies (Fig. 4B and C) in all such cases examined. Furthermore, the polyclonal antibody to TDP-43 stained compact rounded or irregular cytoplasmic inclusions similar to dense bodies reported by Leigh et al. [33], and the dystrophic neurite-like structure in an apical dendrite in some motoneurons in both types of

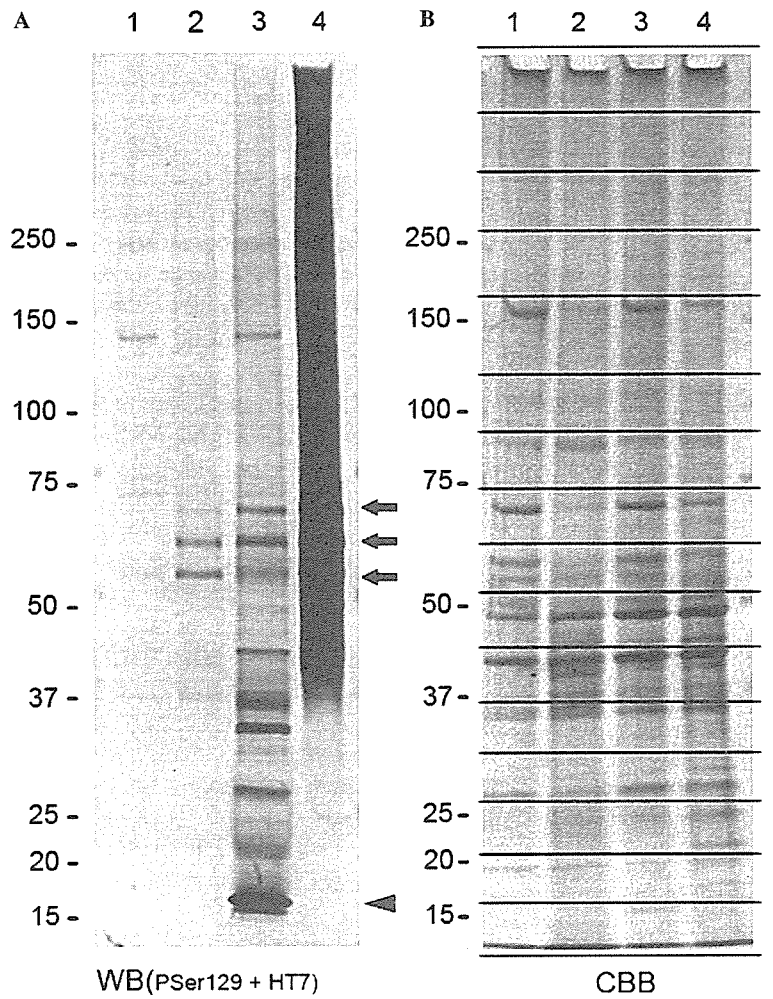

Fig. 1. (A) Immunoblotting of sarkosyl insoluble fraction using a mixture of PSer129 and HT7 antibodies. Lane 1, control (case 37); lane 2, FTLD-MND-type (case 3); lane 3, DLB (case 29); lane 4, AD (case 15). An intense band of α-synuclein in DLB (arrowhead in lane 3) and an abundant triplet of 68, 64, and 60 kDa typical for hyperphosphorylated tau in AD (arrows in lane 4) are shown. There is no positive band in the control (lane A) and only a small amount of triplet of 68, 64, and 60 kDa in FTLD-MND-type (lane 2). (B) Coomassie staining of identical gel to that blotted in (A). Virtually no significant difference is observed among cases (lanes 1–4). Each lane was cut every 5 mm from the bottom to the top of the gel as indicated by horizontal lines for the gel digestion and LC/MS/MS analysis (see Materials and methods for details). Molecular mass markers are shown on the left.

cases (Fig. 4D). In a case of ALS (case 11), neuronal intranuclear inclusions were stained with the polyclonal antibody to TDP-43 in the lumbar and sacral cord (Fig. 4E). Moreover, the polyclonal antibody to TDP-43 stained curved or bullet-shaped inclusions in the cytoplasm of glial cells in the gray matter, and anterior and lateral funiculi of lumber spinal cord in all the ALS and FTLD-MND cases (Fig. 4F and G). Similar glial cytoplasmic inclusions positive for A0024, a phosphorylation-independent antibody to tau, were also found in the same area of the spinal cord (Fig. 4H). The frequency of these inclusions varied from case to case. These TDP-43 positive neuronal intranuclear and glial cytoplasmic inclusions were negative for ubiquitin.

In other diseases, the polyclonal antibody to TDP-43 stained Pick bodies in PiD (Fig. 5A and B), neurofibrillary tangles in AD (Fig. 5C) and tangle only dementia, and thread- or coil-like structures in CBD (Fig. 5D). The number of TDP-43 positive Pick bodies was about comparable to that of tau-positive ones, while only a part of tau-positive structures in AD and CBD were immunopositive for TDP-43. The same antibody did not stain any tau-positive structures in PSP, Lewy bodies in DLB, and glial cytoplasmic inclusions in MSA. The monoclonal antibody to TDP-43 did not stain any structures in these tauopathies and synucleinopathies.

By Western blotting of sarkosyl insoluble fraction using the antibody to TDP-43, a major band of 43 kDa, which might correspond to the full-length TDP-43, was seen in all samples examined. Fig. 6A illustrates the results of Western blotting in the control, DLB, AD, FTLD-MND-type, and FTLD-MND cases. The intensity of the 43-kDa band varied from case to case even among FTLD-MND-type cases (lanes 6–8, 10). However, an additional band of 45 kDa, as well as a diffuse smear staining throughout the gel, was observed only in FTLD-MND-type and FTLD-MND cases (lanes 6–10). Moreover, several positive bands below 40 kDa tend to be more prominent in the

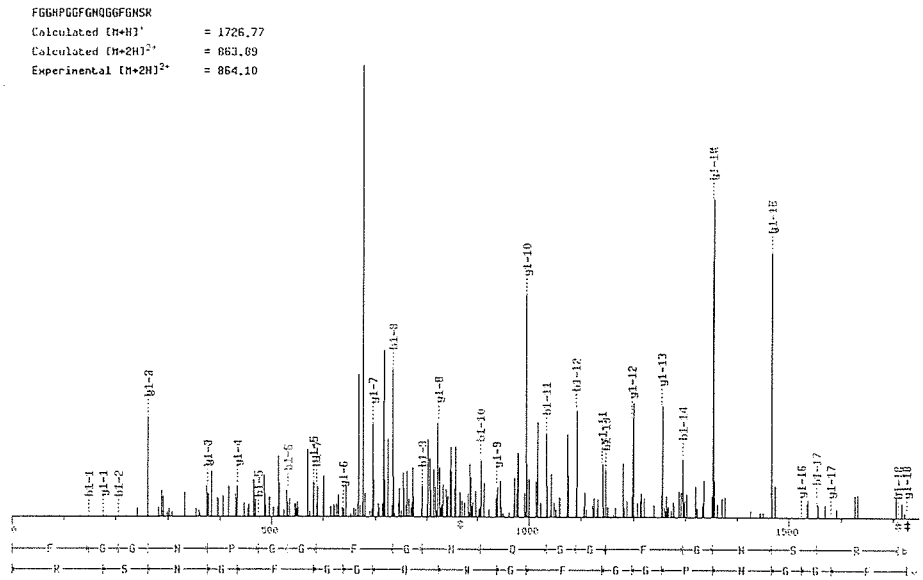

Sequence	#	b	y	(+1)
F	1	148.1	1726.8	18
G	2	205.1	1579.7	17
G	3	262.1	1522.7	16
N	4	376.2	1465.7	15
P	5	473.2	1351.6	14
G	6	530.2	1254.6	13
G	7	587.3	1197.5	12
F	8	734.3	1140.5	11
G	9	791.3	993.5	10
N	10	905.4	936.4	9
Q	11	1033.4	822.4	8
G	12	1090.5	694.3	7
G	13	1147.5	637.3	6
F	14	1294.6	580.3	5
G	15	1351.6	433.2	4
N	16	1465.6	376.2	3
S	17	1552.7	262.2	2
R	18	1708.8	175.1	1

Fig. 2. Identification of a tryptic peptide of TDP-43 in the sarkosyl insoluble fraction extracted from the FTLD-MND-type brain by ion-spray mass spectrometry. Product ion spectrum of mass signal $(M+2H)^{2+}$ of *m/z* 864.10 (the b and y ion series) is shown.

FTLD-MND-type and FTLD-MND than in other cases. After dephosphorylation of the samples, the 45-kDa band disappeared, suggesting that phosphorylation takes place in the full-length TDP-43 (Fig. 6B). Western blotting of the samples from PiD and MSA showed mainly a single band of 43 kDa as in DLB, AD, and the control (data not shown).

Discussion

TDP-43 is a ubiquitously expressed human protein that functions in transcriptional repression and exon skipping. It was first identified as a protein capable of binding to a TAR DNA of the human immunodeficiency virus 1 (HIV-1) long terminal repeat (LTR) region [27]. TDP-43 interacts with several nuclear ribonucleoproteins (RNP) including heterogeneous nuclear RNP A/B and survival motor neuron protein, inhibiting alternative splicing [34,35]. Database analysis and cDNA cloning have shown that the primary transcript of the human TDP gene undergoes alternative splicing to generate 8 mRNA [28]. The physiological function of TDP-43 in brain cells has not yet been determined.

In the present study, we have identified TDP-43 as a component of neuronal and glial inclusions in

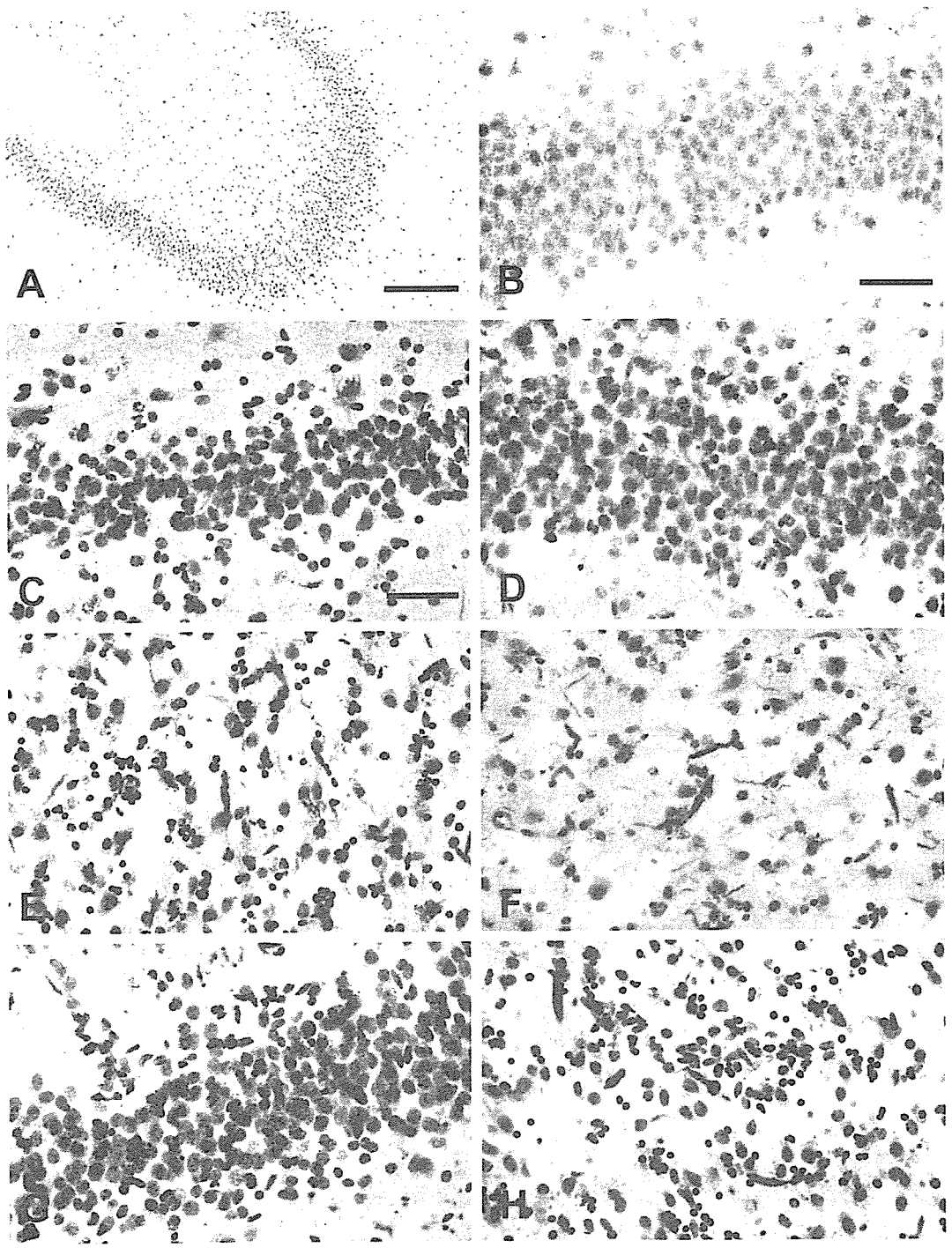

Fig. 3. Immunohistochemical staining of the hippocampal region in FTLD-MND-type with a polyclonal antibody to TDP-43 (A,C,E); a monoclonal antibody to TDP-43 (B,D,F); a monoclonal antibody to ubiquitin (DF2) (G,H). In the control (A,B), both polyclonal (A) and monoclonal (B) antibodies to TDP-43 immunostain the neuronal and glial nuclei in the hippocampus. The nuclear staining of the granular cells in the dentate gyrus is shown in (A and B). In the FTLD-MND-type (C–H), both polyclonal and monoclonal antibodies to TDP-43 stain the cytoplasmic inclusions in the granular cells in the dentate gyrus (C,D) and dystrophic neurites in the parahippocampal cortex (E,F). The morphology of these TDP-43 positive inclusions and neurites is comparable to that of ubiquitin-positive inclusions (G) and neurites (H). The sections are counterstained with hematoxylin to reveal nuclei in (C–H). Scale bars A 200 μm; B 100 μm; C (also for D–H) 50 μm.

FTLD-MND-type, FTLD-MND, and ALS by biochemical and immunohistochemical methods. On Western blotting of sarkosyl insoluble fractions using the antibody to TDP-43, FTLD-MND-type and FTLD-MND cases showed an additional 45-kDa band and diffuse smear staining, phenomena not observed in AD, DLB, PiD, MSA or control cases. Disappearance of the 45-kDa band after dephosphorylation suggests that phosphorylation of full-length TDP-43 takes place. This is important since abnormal phosphorylation of accumulated proteins like tau or

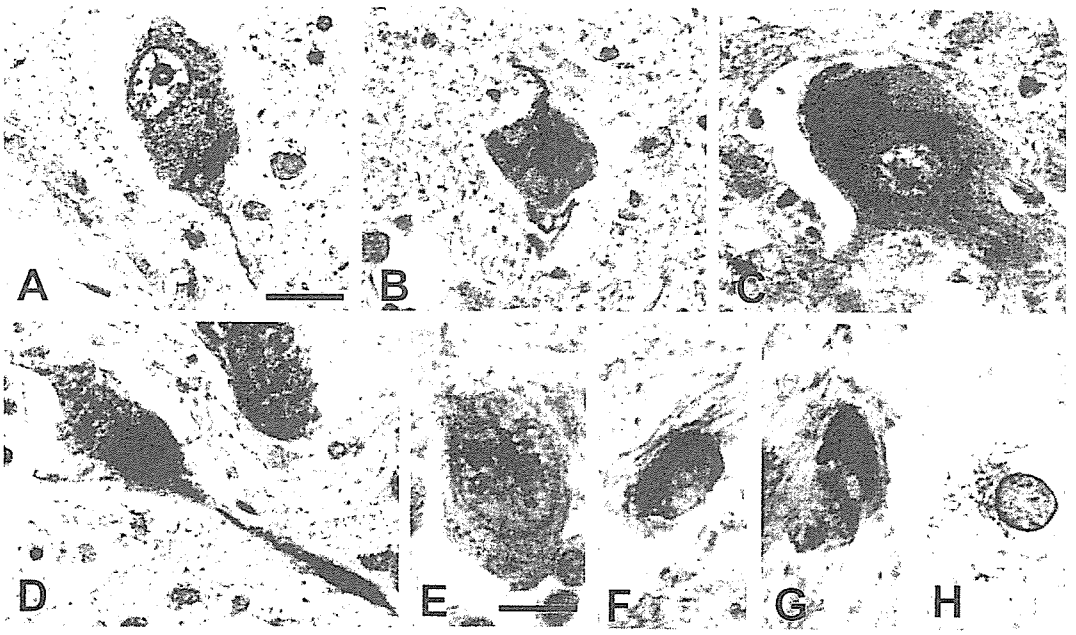

Fig. 4. Immunostaining of the spinal cord in ALS. Skein-like inclusions in the motoneurons of the lumbar spinal cord are stained with anti-ubiquitin (DF2, A) and both polyclonal (B) and monoclonal (C) antibodies to TDP-43. A compact rounded inclusion in a neuronal cytoplasm and the dystrophic neurite-like structure in an apical dendrite are stained with the polyclonal antibody to TDP-43 in the anterior horn of the lumber spinal cord (D). Two neuronal intranuclear inclusions that are positive for TDP-43 are shown in the anterior horn of the sacral cord (E). TDP-43 positive glial inclusions curved (F) or bullet-shaped (G) are observed in the lumbar spinal cord. Similar glial inclusions positive for tau are also found in the lumbar spinal cord (H). The sections are counterstained with hematoxylin. Bars A (also for B–D) 20 μm; D (also for F–H) 8 μm.

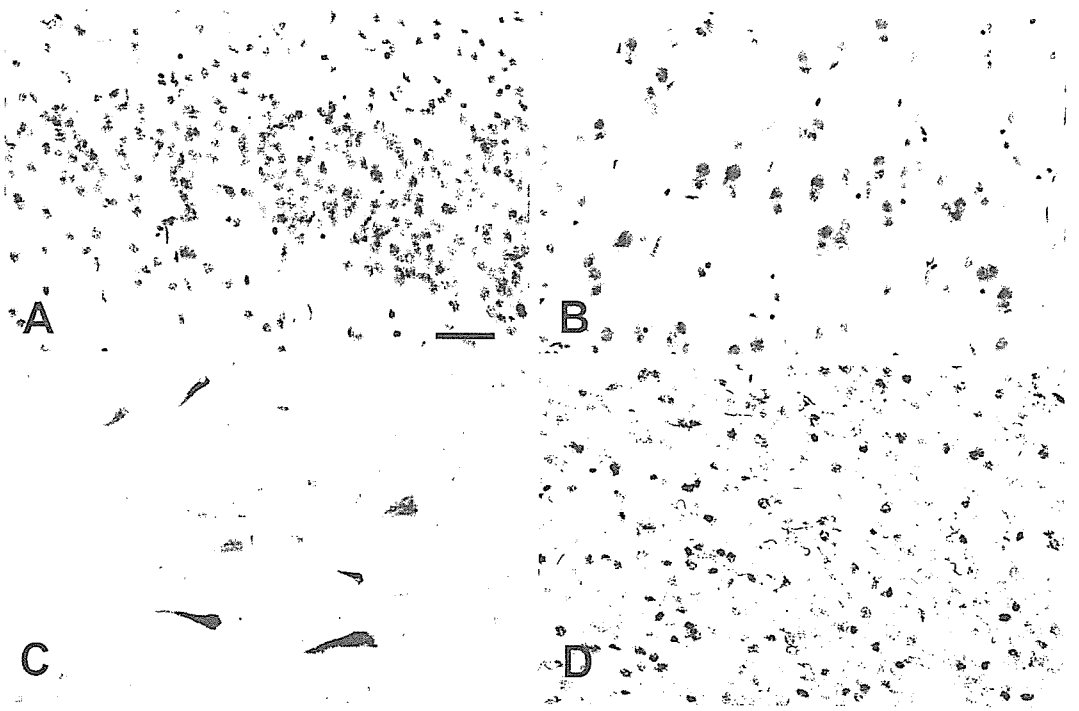

Fig. 5. The polyclonal antibody to TDP-43 stains Pick bodies in the dentate gyrus (A) and the CA1 region (B) of the hippocampus in Pick's disease, neurofibrillary tangles in the CA1 region of the hippocampus in Alzheimer's disease (C), and thread- or coil-like structures in the frontal cortex in corticobasal degeneration (D). The sections are counterstained with hematoxylin in (A and B). The diaminobenzidine reaction is intensified with nickel ammonium sulfate to yield a dark purple precipitate in (D). Thus, most round immunopositive structures in (D) indicate nuclei of neurons and glial cells. Bar A 50 μm.

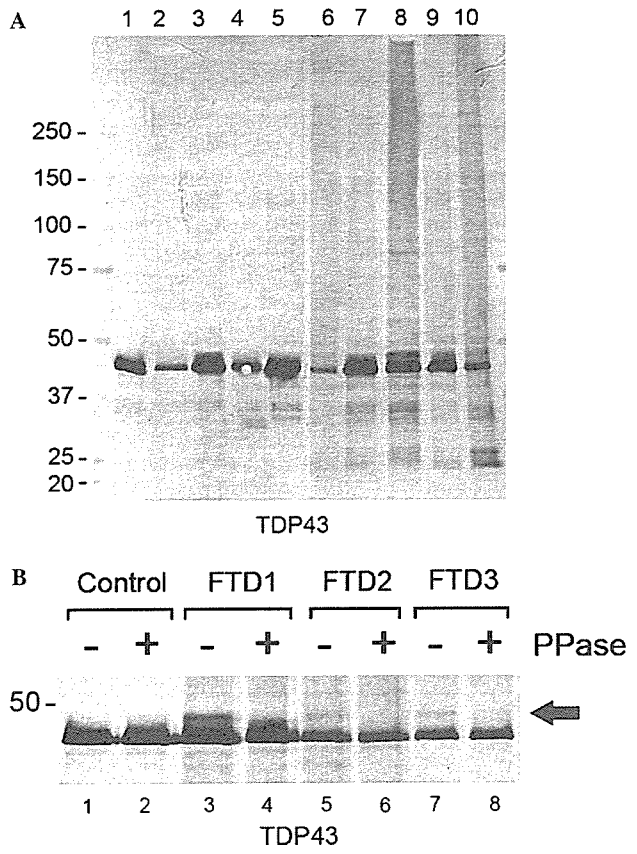

Fig. 6. Immunoblotting of the sarkosyl insoluble fraction with the antibody to TDP-43. (A) Lane 1, control (case 37); lanes 2 and 3, DLB (cases 30, 31); lanes 4 and 5, AD (cases 14, 15); lanes (6–8) and 10, FTLD-MND-type (cases 1–4); lane 9, FTLD-MND (case 7). A positive band of 43 kDa is commonly seen in all cases (lanes 1–10), while an additional band of 45 kDa as well as a diffuse smear staining are observed only in FTLD-MND-type and FTLD-MND (lanes 6–10). Furthermore, several positive bands below 40 kDa are more prominent in FTLD-MND-type and FTLD-MND (lanes 6–10) than in other cases (lanes 1–5). (B) The effect of dephosphorylation on the samples from the control (lanes 1 and 2, case 37) and FTLD-MND-type (lanes 3 and 4, case 3; lanes 5 and 6, case 4; lanes 7 and 8, case 1). Lanes 1, 3, 5, and 7, non-dephosphorylated samples; lanes 2, 4, 6 and 8, dephosphorylated samples. Dephosphorylation does not change the electrical mobility of a major band of 43 kDa in the control (lanes 1, 2) and FTLD-MND-type (lanes 3–8). However, another band of 45 kDa observed in the non-dephosphorylated samples from FTLD-MND-type cases (arrow in lanes 3, 5, 7) is not seen after dephosphorylation (lanes 4, 6, and 8). A faint band of 44 kDa appearing in lane 4 may represent a partial dephosphorylation of the 45-kDa band. Staining was performed with the polyclonal antibody to TDP-43. Molecular mass markers are shown on the left.

α-synuclein has been reported to play an major role in the pathogenesis in many neurodegenerative diseases including AD or Parkinson's disease [30,36]. The smear staining for TDP-43 is also of interest since a similar staining pattern of insoluble tau on immunoblot, referred to as smeared tau, has been reported to be characteristic of tau with abnormal modifications in AD, including phosphorylation, ubiquitination, deamidation, isomerization, and proteolytic cleavage [37–40]. Finally, the TDP-43 positive lower molecular weight bands prominently found in FTLD-MND-type and FTLD-MND cases may represent fragments or alternatively spliced isoforms of TDP-43 [28]. Further analysis is needed to elucidate this issue.

These findings suggest the possibility that an imbalance between kinases and phosphatases is involved in the pathogenesis of these disorders. There is no report indicating such an abnormality in the brain of FTLD-MND-type and FTLD-MND cases. In the spinal cord of ALS patients, however, the elevated expression and/or activation of many protein kinases such as protein kinase C (PKC), glycogen synthase kinase α/β (GSK3α/β), p38 mitogen-activated protein kinase (p38MAPK), calcium/calmodulin-dependent protein kinase kinase (CaMKK), extracellular regulated kinase 2 (ERK2), and stress-activated protein kinase (SAPK) have been shown [41]. Moreover, skein-like inclusions, a specific pathological feature for ALS [32,33], are immunopositive for activated p38MAPK, suggesting that phosphorylation of proteins might be involved in the pathological processes in ALS [42]. Further analysis is needed to clarify the details of abnormal modifications of TDP-43 including phosphorylation sites and responsible kinases.

Immunohistochemical examinations in this study have shown that both polyclonal and monoclonal antibodies to TDP-43 recognize all the pathological hallmarks of FTLD-MND-type, FTLD-MND, and ALS. They include NCI and dystrophic neurites in the hippocampus and temporal cortex in FTLD-MND-type and FTLD-MND, and skein-like inclusions in the spinal cord in FTLD-MND and ALS cases.

In addition, in the spinal cord of FTLD-MND and ALS cases, we have identified some TDP-43 positive structures that have not been reported so far. They include compact and rounded inclusions, neuronal intranuclear inclusions, and glial cytoplasmic inclusions. The morphology of the first is similar to that of dense bodies, which are ubiquitin-positive cytoplasmic inclusions with dense rounded or irregular shape found in the anterior horn cells of ALS patients [33]. However, they showed negative or very weak immunoreactivity for ubiquitin. The distribution of TDP-43 positive glial inclusions was consistent with the degenerating areas including the gray matter of the anterior horn, and anterior and lateral funiculi. These glial inclusions were also positive for tau. Tau-positive glial inclusions have so far been reported in the hippocampus, amygdala, and frontal and temporal lobes in ALS and FTLD-MND [43–45]. Taken together, these findings suggest that glial abnormalities associated with the accumulation of TDP-43 and/or tau may be involved in the pathological process of ALS and FTLD-MND. Regarding neuronal intranuclear inclusions in the ALS patients, eosinophilic and ubiquitin-positive neuronal intranuclear inclusions have been observed in pyramidal neurons of hippocampus and motor cortex, but not in the spinal cord [46,47]. Because of the failure to detect these glial inclusions and neuronal intranuclear inclusions by the monoclonal antibody to TDP-43, the pathological significance of these structures remains to be investigated further.

Similarly, the significance of the immunoreactivities of tau-positive structures in other diseases including Pick

bodies to the polyclonal antibody to TDP-43 is elusive. It is unlikely that the cross reaction of this antibody to tau takes place since it did not recognize tau on immunoblot, although the reactivity of antibody can sometimes differ between in immunoblot and in immunohistochemistry. The lack of biochemical abnormality of TDP-43 in sarkosyl insoluble fraction from AD and PiD brains may suggest that the positive stainings in the sections of these diseases are a nonspecific or secondary phenomenon. We cannot exclude, however, the possibility of the involvement of TDP-43 in the formation of tau-positive structures at present.

Cases of ALS with dementia have been described since 1920s [48]. Recently, accumulating evidences have supported the close association between ALS and FTD. For instance, the incidence of FTD in patients with bulbar onset ALS is as high as 48% [49]. Conversely, 50% of FTD patients meets the criteria of definite or probable ALS [50]. The ALS patients show fronto-temporal pattern of cognitive dysfunction on neuropsychological testing [51]. The number of axons in the pyramidal tract is reduced in FTD patients without MND [13]. A number of families have been described in which different members may develop FTD, FTD with MND or ALS [20,52,53]. The common occurrence of intracellular TDP-43 accumulations in FTLD-MND-type, FTLD-MND, and ALS further supports the hypothesis that these disorders represent a clinicopathological spectrum of a single disease. It can be proposed that they be newly classified as a proteinopathy of TDP-43.

Note added in proof

After we submitted this report, similar observations were reported by Neumann et al. (Science 314 (2006) 130–133).

Acknowledgments

We thank Dr. F. Kametani for assistance in mass spectrometric analysis, and Drs. T. Odawara and E. Iseki for providing brain tissues.

References

[1] G.M. McKhann, M.S. Albert, M. Grossman, B. Miller, D. Dickson, J.Q. Trojanowski, Clinical and pathological diagnosis of frontotemporal dementia: report of the work group on frontotemporal dementia and Pick's disease, Arch. Neurol. 58 (2001) 1803–1809.

[2] Y. Mitsuyama, S. Takamiya, Presenile dementia with motor neuron disease in Japan. A new entity? Arch. Neurol. 36 (1979) 592–593.

[3] I. Nakano, Temporal lobe lesions in amyotrophic lateral sclerosis with dementia-lesions in the apical cortex and some deeper structures of the temporal lobes, Neuropathology 12 (1992) 69–77.

[4] G. Wightman, V.E.R. Anderson, A.J. Martin, M. Swash, B.H. Anderson, D. Neary, D. Mann, P. Luthert, P.N. Leigh, Hippocampal and neocortical ubiquitin-immunoreactive inclusions in amyotrophic lateral sclerosis with dementia, Neurosci. Lett. 139 (1992) 269–274.

[5] M. Jackson, G. Lennox, J. Lowe, Motor neuron disease-inclusion dementia, Neurodegeneration 5 (1996) 339–350.

[6] E. Iseki, F. Li, T. Odawara, H. Hino, K. Suzuki, K. Kosaka, H. Akiyama, K. Ikeda, M. Kato, Ubiquitin-immunohistochemical investigation of atypical Pick's disease without Pick bodies, J. Neurol. Sci. 159 (1998) 194–201.

[7] K. Ikeda, Neuropathological discrepancy between Japanese Pick's disease without Pick bodies and frontal lobe degeneration type of frontotemporal dementia proposed by Lund and Manchester group, Neuropathology 20 (2000) 76–82.

[8] D.S. Knopman, A.R. Mastri, W.H. Frey, J.H. Sung, T. Rustan, Dementia lacking distinctive histologic features: a common non-Alzheimer degenerative dementia, Neurology 40 (1990) 251–256.

[9] A.M. Lipton, C.L. White III, E.H. Bigio, Frontotemporal lobar degeneration with motor neuron disease-type inclusions predominates in 76 cases of frontotemporal degeneration, Acta Neuropathol. (Berl.) 108 (2004) 379–385.

[10] K. Okamoto, S. Hirai, T. Yamazaki, X. Sun, Y. Nakazato, New ubiquitin-positive intraneuronal inclusions in the extra-motor cortices in patients with amyotrophic lateral sclerosis, Neurosci. Lett. 129 (1991) 233–236.

[11] K. Okamoto, N. Murakami, H. Kusada, M. Yoshida, Y. Hashizume, Y. Nakazato, E. Matsubara, S. Hirai, Ubiquitin-positive intraneuronal inclusions in the extramotor cortices of presenile dementia patients with motor neuron disease, J. Neurol. 239 (1992) 426–430.

[12] M. Bergmann, K. Kuchelmeister, K.W. Schmid, H.A. Kretzschmar, R. Schröder, Different variants of frontotemporal dementia: a neuropathological and immunohistochemical study, Acta Neuropathol. (Berl.) 92 (1996) 170–179.

[13] K. Ikeda, H. Akiyama, T. Arai, H. Ueno, K. Tsuchiya, K. Kosaka, Morphometrical reappraisal of motor neuron system of Pick's disease and amyotrophic lateral sclerosis with dementia, Acta Neuropathol. (Berl.) 104 (2002) 21–28.

[14] I.R.A. Mackenzie, H.H. Feldman, Ubiquitin immunohistochemistry suggests classic motor neuron disease, motor neuron disease with dementia, and frontotemporal dementia of the motor neuron disease type represent a clinicopathological spectrum, J. Neuropathol. Exp. Neurol. 64 (2005) 730–739.

[15] T. Arai, T. Nonaka, M. Hasegawa, H. Akiyama, M. Yoshida, Y. Hashizume, K. Tsuchiya, T. Oda, K. Ikeda, Neuronal and glial inclusions in frontotemporal dementia with or without motor neuron disease are immunopositive for p62, Neurosci. Lett. 342 (2003) 41–44.

[16] F. Mori, M. Nishie, Y.S. Piao, K. Kito, T. Kamitani, H. Takahashi, K. Wakabayashi, Accumulation of NEDD8 in neuronal and glial inclusions of neurodegenerative disorders, Neuropathol. Appl. Neurobiol. 31 (2005) 53–61.

[17] E. Kuusisto, A. Salminen, I. Alafuzoff, Ubiquitin-binding protein p62 is present in neuronal and glial inclusions in human tauopathies and synucleinopathies, Neuroreport 12 (2001) 2085–2090.

[18] S.M. Rosso, W. Kamphorst, G. de Graaf, R. Willemsen, R. Ravid, M.F. Niermeijer, M.G. Spillantini, P. Heutink, J.C. van Swieten, Familial frontotemporal dementia with ubiquitin-positive inclusions is linked to chromosome 17q21-22, Brain 124 (2001) 1948–1957.

[19] J. Woulfe, A. Kertesz, D.G. Munoz, Frontotemporal dementia with ubiquitinated cytoplasmic and intranuclear inclusions, Acta Neuropathol. (Berl.) 102 (2001) 94–102.

[20] C. Vance, A. Al-Chalabi, D. Ruddy, B.N. Smith, X. Hu, J. Sreedharan, T. Siddique, H.J. Schelhaas, B. Kusters, D. Troost, F. Baas, V. de Jong, C.E. Shaw, Familial amyotrophic lateral sclerosis with frontotemporal dementia is linked to a locus on chromosome 9p13.2-21.3, Brain 129 (2006) 868–875.

[21] M.S. Forman, I.R. Mackenzie, N.J. Cairns, E. Swanson, P.J. Boyer, D.A. Drachman, B.S. Jhaveri, J.H. Karlawish, A. Pestronk, T.W. Smith, P. Tu, G.D.J. Watts, W.R. Markesbery, C.D. Smith, V.E. Kimonis, Novel ubiquitin neuropathology in frontotemporal dementia with valosin-containing protein gene mutations, J. Neuropathol. Exp. Neurol. 65 (2006) 571–581.

[22] M. Cruts, I. Gijselinck, J. van der Zee, S. Engelborghs, H. Wils, D. Pirici, R. Rademakers, R. Vandenberghe, B. Dermaut, J. Martin, C.

van Duijin, K. Peeters, R. Sciot, P. Santens, T. De Pooter, M. Mattheijssens, M. Van den Broeck, I. Cuijt, K. Vennekens, P.P. De Deyn, S. Kumar-Singh, C. Van Broeckhoven, Null mutations in progranulin cause ubiquitin-positive frontotemporal dementia linked to chromosome 17q21, Nature 442 (2006) 920–924.

[23] M. Baker, I.R. Mackenzie, S.M. Pickering-Brown, J. Gass, R. Rademakers, C. Lindholm, J. Snowden, J. Adamson, A.D. Sadovnick, S. Rollinson, A. Cannon, E. Dwosh, D. Neary, S. Melquist, A. Richardson, D. Dickson, Z. Berger, J. Eriksen, T. Robinson, C. Zehr, C.A. Dickey, R. Crook, E. McGowan, D. Mann, B. Boeve, H. Feldman, M. Hutton, Mutations in progranulin cause tau-negative frontotemporal dementia linked to chromosome 17, Nature 442 (2006) 916–919.

[24] O. Mukherjee, P. Pastor, N.J. Cairns, S. Chakraverty, J.S.K. Kauwe, S. Shears, M.I. Behrens, J. Budde, A.L. Hinrichs, J. Norton, D. Levitch, L. Taylor-Reinwald, M. Gitcho, P.-H. Tu, L.T. Grinberg, R.M. Liscic, J. Armendariz, J.C. Morris, A.M. Goate, HDDD2 is a familial frontotemporal lobar degeneration with ubiquitin-positive tau-negative inclusions caused by a missense mutation in the signal peptide of progranulin, Ann. Neurol. 60 (2006) 314–322.

[25] J. Gass, A. Cannon, I.R. Mackenzie, B. Boeve, M. Baker, J. Adamson, R. Crook, S. Melquist, K. Kuntz, R. Peterson, K. Josephs, S.-P. Brown, N. Graff-Radford, R. Uitti, D. Dickson, Z. Wzsolek, J. Gonzalez, T.G. Beach, E. Bigio, N. Johnson, S. Weintraub, M. Mesulam, C.L. White III, B. Woodruff, R. Caselli, G.-Y. Hsiung, H. Feldman, D. Knopman, M. Hutton, R. Rademakers, Mutations in progranulin are a major cause of ubiquitin-positive frontotemporal lobar degeneration, Hum. Mol. Genet., advance online publication, doi:10.1093/hmg/ddl241 (2006).

[26] G.D.J. Watts, J. Wymer, M.J. Kovach, S.G. Mehta, S. Mumm, D. Darvish, A. Pestronk, M.P. Whyte, V.E. Kimonis, Inclusion body myopathy associated with Paget disease of bone and frontotemporal dementia is caused by mutant valosin-containing protein, Nat. Genet. 36 (2004) 377–381.

[27] S.H. Ou, F. Wu, D. Harrich, L.F. García-Martínez, R.B. Gaynor, Cloning and characterization of a novel cellular protein, TDP-43, that binds to human immunodeficiency virus type 1 TAR DNA sequence motifs, J. Virol. 69 (1995) 3584–3596.

[28] H.-Y. Wang, I.-F. Wang, J. Bose, C.-K.J. Shen, Structural diversity and functional implications of the eukaryotic TDP gene family, Genomics 83 (2004) 130–139.

[29] H. Mori, J. Kondo, Y. Ihara, Ubiquitin is a component of paired helical filaments in Alzheimer's disease, Science 235 (1987) 1641–1644.

[30] H. Fujiwara, M. Hasegawa, N. Dohmae, A. Kawashima, E. Masliah, M.S. Goldberg, J. Shen, K. Takio, T. Iwatsubo, α-Synuclein is phosphorylated in synucleinopathy lesions, Nat. Cell. Biol. 4 (2002) 160–164.

[31] M. Goedert, M.G. Spillantini, N.J. Cairns, R.A. Crowther, Tau proteins of Alzheimer paired helical filaments: abnormal phosphorylation of all six brain isoforms, Neuron 8 (1992) 159–168.

[32] J. Lowe, G. Lennox, D. Jefferson, K. Morrell, D. McQuire, T. Gray, M. Landon, F.J. Doherty, R.J. Mayer, A filamentous inclusion body within anterior horn neurones in motor neurone disease defined by immunocytochemical localization of ubiquitin, Neurosci. Lett. 94 (1988) 203–210.

[33] P.N. Leigh, H. Whitwell, O. Garofalo, J. Buller, M. Swash, J.E. Martin, J.-M. Gallo, R.O. Weller, B.H. Anderton, Ubiquitin-immunoreactive intraneuronal inclusions in amyotrophic lateral sclerosis, Brain 114 (1991) 775–788.

[34] E. Buratti, A. Brindisi, M. Giombi, S. Tisminetzky, Y.M. Ayala, F.E. Baralle, TDP-43 binds heterogeneous nuclear ribonucleoprotein A/B through its C-terminal tail, J. Biol. Chem. 280 (2005) 37572–37584.

[35] I.-F. Wang, N.M. Reddy, C.-K.J. Shen, Higher order arrangement of the eukaryotic nuclear bodies, Proc. Natl. Acad. Sci. USA 99 (2002) 13583–13588.

[36] M. Hasegawa, M. Morishima-Kawashima, K. Takio, M. Suzuki, K. Titani, Y. Ihara, Protein sequence and mass spectrometric analyses of tau in the Alzheimer's disease brain, J. Biol. Chem. 267 (1992) 17047–17054.

[37] Y. Ihara, C. Abraham, D.J. Selkoe, Antibodies to paired helical filaments in Alzheimer's disease do not recognize normal brain proteins, Nature 304 (1983) 727–730.

[38] R. Endoh, M. Ogawara, T. Iwatsubo, I. Nakano, H. Mori, Lack of the carboxyl terminal sequence of tau in ghost tangle of Alzheimer's disease, Brain Res. 601 (1993) 164–172.

[39] A. Watanabe, K. Takio, Y. Ihara, Deamidation and isoaspartate formation in smeared tau in paired helical filaments, J. Biol. Chem. 274 (1999) 7368–7378.

[40] T. Arai, K. Ikeda, H. Akiyama, K. Tsuchiya, S. Iritani, K. Ishiguro, S. Yagishita, T. Oda, T. Odawara, E. Iseki, Different immunoreactivities of the microtubule-binding region of tau and its molecular basis in brains from patients with Alzheimer's disease, Pick's disease, progressive supranuclear palsy and corticobasal degeneration, Acta Neuropathol. (Berl.) 105 (2003) 489–498.

[41] J.H. Hu, H. Zhang, R. Wagey, C. Krieger, S.L. Pelech, Protein kinase and protein phosphatase expression in amyotrophic lateral sclerosis spinal cord, J. Neurochem. 85 (2003) 432–442.

[42] C. Bendotti, C. Atzori, R. Piva, M. Tortarolo, M.J. Strong, S. Debiasi, A. Migheli, Activated p38MAPK is a novel component of the intracellular inclusions found in human amyotrophic lateral sclerosis and mutant SOD1 transgenic mice, J. Neuropathol. Exp. Neurol. 63 (2004) 113–119.

[43] K. Noda, S. Katayama, C. Watanabe, Y. Yamamura, S. Nakamura, Gallyas- and tau-positive glial structures in motor neuron disease with dementia, Clin. Neuropathol. 18 (1999) 218–225.

[44] L.S. Forno, J.W. Langston, M.K. Herrick, J.D. Wilson, S. Murayama, Ubiquitin-positive neuronal and tau 2-positive glial inclusions in frontotemporal dementia of motor neuron type, Acta Neuropathol. (Berl.) 103 (2002) 599–606.

[45] W. Yang, M.M. Sopper, C. Leystra-Lanz, M.J. Strong, Microtubule-associated tau protein positive neuronal and glial inclusions in ALS, Neurology 61 (2003) 1766–1773.

[46] A. Kakita, K. Oyanagi, H. Nagai, H. Takahashi, Eosinophilic intranuclear inclusions in the hippocampal pyramidal neurons of a patient with amyotrophic lateral sclerosis, Acta Neuropathol. (Berl.) 93 (1997) 532–536.

[47] D. Seilhean, J. Takahashi, K.H. El Hachimi, H. Fujigasaki, A.-S. Lebre, V. Biancalana, A. Dürr, F. Salachas, J. Hogenhuis, H. de Thé, J.-J. Hauw, V. Meininger, A. Brice, C. Duyckaerts, Amyotrophic lateral sclerosis with neuronal intranuclear protein inclusions, Acta Neuropathol. (Berl.) 108 (2004) 81–87.

[48] A.J. Hudson, Amyotrophic lateral sclerosis and its association with dementia, parkinsonism and other neurological disorders: a review, Brain 104 (1981) 217–247.

[49] F. Portet, C. Cadihac, J. Touchon, W. Camu, Cognitive impairment in motor neuron disease with bulbar onset, Amyotroph. Lateral Scler. Other Motor Neuron Disord. 2 (2001) 23–29.

[50] C. Lomen-Hoerth, T. Anderson, B. Miller, The overlap of amyotrophic lateral sclerosis and frontotemporal dementia, Neurology 59 (2002) 1077–1079.

[51] H. Schreiber, T. Gaigalat, U. Wiedemuth-Catrinescu, M. Graf, I. Uttner, R. Muche, A.C. Ludolph, Cognitive function in bulbar- and spinal-onset amyotrophic lateral sclerosis. A longitudinal study in 52 patients, J. Neurol. 252 (2005) 772–781.

[52] B.A. Hosler, T. Siddique, P.C. Sapp, W. Sailor, M.C. Huang, A. Hossain, J.R. Daube, M. Nance, C. Fan, J. Kaplan, W.-Y. Hung, D. McKenna-Yasek, J.L. Haines, M.A. Pericak-Vance, H.R. Horvitz, R.H. Brown Jr., Linkage of familial amyotrophic lateral sclerosis with frontotemporal dementia to chromosome 9q21-q22, JAMA 284 (2000) 1664–1669.

[53] M. Morita, A. Al-Chalabi, P.M. Anderson, B. Hosler, P. Sapp, E. Englund, J.E. Mitchell, J.J. Habgood, J. de Belleroche, J. Xi, W. Jongjaroenprasert, H.R. Horvitz, L.-G. Gunnarsson, R.H. Brown Jr., A locus on chromosome 9p confers susceptibility to ALS and frontotemporal dementia, Neurology 66 (2006) 839–844.

THE JOURNAL OF BIOLOGICAL CHEMISTRY VOL. 281, NO. 44, pp. 33250–33257, November 3, 2006

Dyrk1A Phosphorylates α-Synuclein and Enhances Intracellular Inclusion Formation*

Received for publication, June 27, 2006, and in revised form, September 6, 2006 Published, JBC Papers in Press, September 7, 2006, DOI 10.1074/jbc.M606147200

Eun Joo Kim[‡], Jee Young Sung[§], Hyun Jung Lee[‡], Hyewhon Rhim[¶], Masato Hasegawa[‖], Takeshi Iwatsubo[**], Do Sik Min[‡‡], Jongsun Kim[§§], Seung R. Paik[¶¶], and Kwang Chul Chung[‡1]

From the [‡]Department of Biology, College of Science, Yonsei University, Seoul 120-749, Korea, the Departments of [§]Medical Science and [§§]Microbiology, Yonsei University College of Medicine, Seoul 120-752, Korea, the [¶¶]School of Chemical and Biological Engineering, College of Engineering, Seoul National University, Seoul 151-744, Korea, [¶]Biomedical Research Center, Korea Institute of Science and Technology, Seoul 136-701, Korea, the [‡‡]Department of Molecular Biology, College of Natural Science, Pusan National University, Busan 609-735, Korea, [‖]Tokyo Institute of Psychiatry, Tokyo 156-8585, Japan, and the [**]Department of Neuropathology and Neuroscience, University of Tokyo, Tokyo 113-0033, Japan

Lewy bodies (LBs) are pathological hallmarks of Parkinson disease (PD) but also occur in Alzheimer disease (AD) and dementia of LBs. α-Synuclein, the major component of LBs, is observed in the brain of Down syndrome (DS) patients with AD. Dyrk1A, a dual specificity tyrosine-regulated kinase (Dyrk) family member, is the mammalian ortholog of the *Drosophila minibrain* (*Mnb*) gene, essential for normal postembryonic neurogenesis. The *Dyrk1A* gene resides in the human chromosome 21q22.2 region, which is associated with DS anomalies, including mental retardation. In this study, we examined whether Dyrk1A interacts with α-synuclein and subsequently affects intracellular α-synuclein inclusion formation in immortalized hippocampal neuronal (H19-7) cells. Dyrk1A selectively binds to α-synuclein in transformed and primary neuronal cells. α-Synuclein overexpression, followed by basic fibroblast growth factor-induced neuronal differentiation, resulted in cell death. We observed that accompanying cell death was increased α-synuclein phosphorylation and intracytoplasmic aggregation. In addition, the transfection of kinase-inactive Dyrk1A or Dyrk1A small interfering RNA blocked α-synuclein phosphorylation and aggregate formation. *In vitro* kinase assay of anti-Dyrk1A immunocomplexes demonstrated that Dyrk1A could phosphorylate α-synuclein at Ser-87. Furthermore, aggregates formed by phosphorylated α-synuclein have a distinct morphology and are more neurotoxic compared with aggregates composed of unmodified wild type α-synuclein. These findings suggest α-synuclein inclusion formation regulated by Dyrk1A, potentially affecting neuronal cell viability.

α-Synuclein is a major component of Lewy bodies (LBs)[2] found in Parkinson disease (PD), dementia with LB, Alzheimer disease (AD), and multiple system atropy (1). In these neurodegenerative disorders (collectively referred to as synucleinopathies), LBs are characterized by fibrillar, cytoplasmic α-synuclein aggregates within selective populations of neurons and glial cells (2). α-Synuclein inclusion formation is clearly involved in the pathogenic process of PD. α-Synuclein was first identified as a partial fragment in AD amyloid plaques (41), and subsequently three missense mutations in the α-synuclein gene were reported in early onset familial PD of some kindred (3, 4).

Down syndrome (DS) is the most common genetic disorder, with a frequency of 1 in every 700 – 800 live births, and is caused by an extra copy of all or part of chromosome 21 (5). In addition to characteristic physical features, DS individuals have congenital heart defects, gastrointestinal malformations, immune and endocrine system defects, a high incidence of leukemia, and early onset of Alzheimer-like dementia. DS individuals also exhibit mild to severe mental retardation (6 – 8). Efforts to isolate the gene(s) responsible for DS mental retardation identified *Dyrk1A* as a candidate gene (9, 10).

The *Drosophila melanogaster minibrain* (*Mnb*) gene encodes a serine/threonine protein kinase essential in cell proliferation and neuronal differentiation during postembryonic neurogenesis (10). Dual specificity tyrosine-regulated kinase-1A (*Dyrk1A*), the *Mnb* kinase human homolog, maps to the DS critical region on chromosome 21. *Dyrk1A* is thought to be responsible for the DS neurological defects. In DS fetal brains, *Dyrk1A* expression increases 1.5-fold, and transgenic mice overexpressing *Dyrk1A* exhibit neurodevelopmental delays, motor abnormalities, and cognitive deficits (11, 12).

α-Synuclein post-translational modifications include nitration, glycosylation, and phosphorylation and are likely to influence α-synuclein aggregation. Constitutive α-synuclein phosphorylation at C-terminal Ser-87 and Ser-129 residues occurs in neuronal and nonneuronal cell lines (13). α-Synuclein aggregates in brain tissue from individuals with synucleinopathy are extensively phosphorylated at Ser-129 (14). Furthermore,

* This study was supported by Brain Research Center of the 21st Century Frontier Research Program Grant M103KV010011-06K2201-01110 (to K. C. C.), funded by the Ministry of Science and Technology of Republic of Korea, by Korea Research Foundation Basic Science Research Grant KRF2003-015-C00527 (to K. C. C.), by Korea Health 21 R&D Project, Ministry of Health and Welfare, Republic of Korea, Grants A050181 and A060440 (to K. C. C.), and by Korea Science and Engineering Foundation Basic Research Grant R01-2004-000-10673-0 (to K. C. C.). It was also partly supported by Korea Research Foundation Grant KRF-2004-005-E00017 funded by the Korean Government (to K. C. C). The costs of publication of this article were defrayed in part by the payment of page charges. This article must therefore be hereby marked "*advertisement*" in accordance with 18 U.S.C. Section 1734 solely to indicate this fact.

[1] To whom correspondence should be addressed: Dr. Kwang Chul Chung, Dept. of Biology, College of Science, Yonsei University, Shinchon-dong 134, Seodaemun-gu, Seoul 120-749, Korea. Tel.: 82-2-2123-2653; Fax: 82-2-312-5657; E-mail: kchung@yonsei.ac.kr.

[2] The abbreviations used are: LB, Lewy body; AD, Alzheimer disease; bFGF, basic fibroblast growth factor; DS, Down syndrome; GST, glutathione *S*-transferase; PD, Parkinson disease; HA, hemagglutinin; CREB, cAMP-response element-binding protein.

α-synuclein Ser-129 phosphorylation promotes eosinophilic fibril formation *in vitro* and in SH-SY5Y cells (14, 15). α-Synuclein is a substrate for G protein-coupled receptor kinases, and the protein-tyrosine kinase Pyk2/RAFTK phosphorylates α-synuclein at the Tyr-125 residue in response to hyperosmotic stress (16, 17). These findings suggest that filamentous protein phosphorylation, including α-synuclein phosphorylation, is important in the pathogenesis of neurodegenerative disorders.

Interestingly, α-synuclein-positive LBs and neuritic processes frequently occur in DS brains with AD phenotypes (18). In addition, LB formation frequency in DS patient brains with AD is greater than in sporadic AD cases (19). To study the molecular mechanisms leading to LB formation in DS patients, we examined whether Dyrk1A interacts with α-synuclein and affects cytoplasmic inclusion formation in hippocampal neuroprogenitor cells. Our data show that Dyrk1A phosphorylates α-synuclein at the Ser-87 residue. Additionally, Dyrk1A-mediated α-synuclein phosphorylation facilitates its aggregation.

EXPERIMENTAL PROCEDURES

Materials—Peroxidase-conjugated anti-rabbit and anti-mouse IgGs were purchased from Zymed Laboratories Inc. (San Francisco, CA); Dulbecco's modified Eagle's medium, fetal bovine serum, Lipofectamine Plus reagent, and cell culture reagents were from Invitrogen; glutathione-Sepharose 4B and Protein A-Sepharose were from Amersham Biosciences; ECL reagents and [γ-^{32}P]ATP were from PerkinElmer Life Sciences; anti-α-synuclein IgG was from AbCam; anti-Dyrk1A antibodies were from Santa Cruz Biotechnology, Inc. (Santa Cruz, CA); and anti-phosphoserine/phosphothreonine and anti-tyrosine antibodies were from Sigma. Anti-phospho-Ser-129 α-synuclein antibody was developed as described previously (14). Plasmids encoding HA-tagged Dyrk1A (pSVL-HA-Dyrk1A) and its K188R mutant (pSVL-HA-Dyrk1A-K188R) were kindly provided by W. Becker (Institute of Pharmacology and Toxicology, RWTH, Aachen, Germany). Wild type α-synuclein plasmid was provided by R. Jakes (Medical Research Council Laboratory of Molecular Biology, Cambridge, UK). FLAG-tagged α-synuclein with a serine to alanine point mutation (S9A, S42A, S87A, and S129A) cDNAs were generously provided by C. A. Ross (Johns Hopkins University School of Medicine, Baltimore, MD) and J. L. Benovic (Thomas Jefferson University, Philadelphia, PA). Bacterially recombinant α-synuclein proteins were either purchased from ATGen (Seongnam-si, Gyeonggi-do, Korea) or purified as described previously (20).

Cell Culture and DNA Transfection—Conditionally immortalized hippocampal (H19-7) cell lines were cultured as described previously (21). The neuroblastoma SH-SY5Y cells were maintained in Dulbecco's modified Eagle's medium containing 10% fetal bovine serum with penicillin and streptomycin. Rat fetal brain lysates and primary cortical neurons were prepared as described previously (22). The cells were transfected with Lipofectamine Plus reagent (Invitrogen), according to the supplier's instructions. To prepare cell lysates, cells were rinsed with ice-cold phosphate-buffered saline and solubilized in lysis buffer (10 mM Tris, pH 7.9, containing 1.0% Nonidet P-40, 150 mM NaCl, 1 mM EGTA, 1 mM EDTA, 10% glycerol, 1 mM Na_3VO_4, 1 μg/ml leupeptin, 1 μg/ml aprotinin, 10 mM NaF, and 0.2 mM phenylmethylsulfonyl fluoride). Cells were scraped, and supernatants were collected after centrifugation for 10 min at 14,000 × *g* at 4 °C. Protein concentrations were determined using the detergent-compatible protein assay kit (Bio-Rad).

Cell Viability—Cell survival quantitation was performed using the tetrazolium salt, 3-(4,5-dimethylthiazol-2-yl)-2,5-diphenyltetrazolium bromide extraction method, as described previously (23). Statistical analyses were completed with the aid of the StatView II program (Abacus Concepts, CA). All data were analyzed by one-way analysis of variance and preplanned comparisons with the control were performed by means of Dunnett's T-statistic.

Immunoprecipitation and Western Blot Analysis—One microgram of suitable antibodies was incubated with 0.5–1 mg of cell extracts in cell lysis buffer overnight at 4 °C. Fifty microliters of a 1:1 protein A-Sepharose bead suspension was added and incubated for 2 h at 4 °C with gentle rotation. Beads were pelleted and washed extensively with cell lysis buffer. Bound proteins were dissociated by boiling in SDS-PAGE sample buffer, and samples were separated on SDS-polyacrylamide gel and transferred to a nitrocellulose membrane (Millipore). Membranes were blocked in TBST buffer (20 mM Tris, pH 7.6, 137 mM NaCl, 0.05% Tween 20) plus 3% nonfat dry milk for 3 h and then incubated overnight at 4 °C in TBST buffer with 3% nonfat dry milk and the appropriate antibodies. Membranes were washed several times in TBST and then incubated with secondary IgG-coupled horseradish peroxidase antibody (Zymed Laboratories Inc.). After 60 min, the blots were washed several times with TBST and visualized by ECL.

Immunocytochemistry—Cells were seeded overnight, at 70% confluence, onto coverslips in 6-well dishes and transfected with the appropriate plasmids the following day for 24 h. After washing with phosphate-buffered saline, the cells were fixed with neutral buffered 4% (w/v) paraformaldehyde and permeabilized with 1% bovine serum albumin containing 0.1% Triton X-100 for 1 h. Cells were incubated at 4 °C for 24 h with the appropriate primary antibody and diluted in phosphate-buffered saline containing 1% bovine serum albumin. After washing with phosphate-buffered saline, either rhodamine- or fluorescein isothiocyanate-coupled secondary antibodies were added and incubated for 2 h at room temperature. Fixed cells were analyzed by confocal or fluorescence microscopy.

Hematoxylin and Eosin Staining—Hematoxylin and eosin staining were performed according to the manufacturer's instructions (Sigma). We counted cells with eosinophilic inclusions in six different fields, ~1000 cells/experimental condition.

In Vitro Kinase Assay—Confluent cells were harvested in lysis buffer. Soluble cell lysate fraction was incubated for 2 h at 4 °C with suitable antibodies. After the addition of protein A-Sepharose beads, the reaction mixture was incubated for 2 h at 4 °C and rinsed with lysis and kinase buffers. Immunocomplex kinase assays were performed by incubating the cell lysates for 2 h at 30 °C with the substrate in the reaction buffer (0.2 mM sodium orthovanadate, 2 mM dithiothreitol, 10 mM $MgCl_2$, 2 mCi of [γ-^{32}P]ATP, and 20 mM HEPES, pH

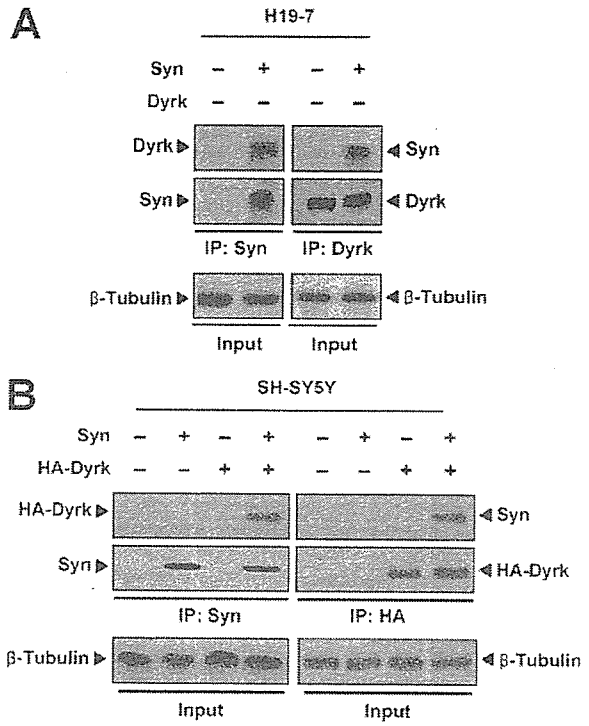

FIGURE 1. **Dyrk1A binds to α-synuclein in hippocampal H19-7 cells and neuroblastoma SH-SY5Y cells.** *A*, H19-7 cell lines were mock-transfected (−) or transiently transfected with α-synuclein (*Syn*). After 24 h, immunoprecipitation (*IP*) was performed with either anti-α-synuclein or anti-Dyrk1A antibodies and subsequently examined by Western blot analysis with anti-Dyrk1A or anti-α-synuclein antibodies. β-Tubulin expression showed equal loading. *B*, α-Synuclein (*Syn*) or HA-tagged Dyrk1A was transfected separately or together into SH-SY5Y cells. Immunoprecipitation was performed with either anti-α-synuclein or anti-HA antibodies, and the immunocomplexes were analyzed by Western blot analysis with either anti-HA or anti-α-synuclein antibodies. These results are representative of three independent experiments.

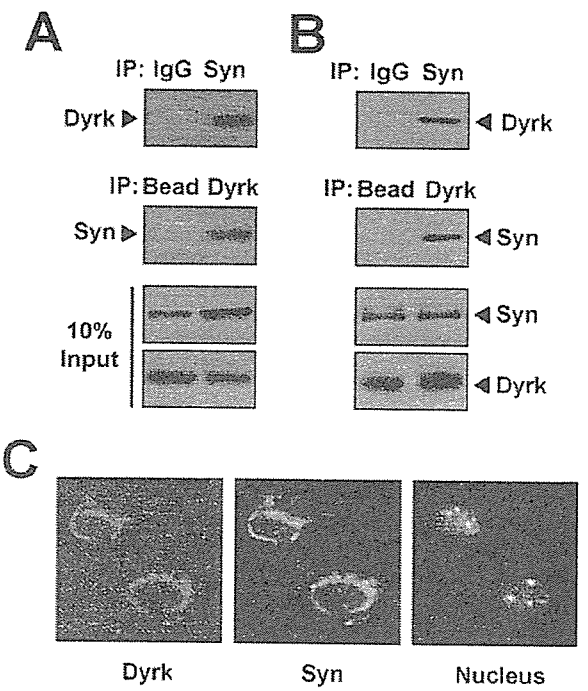

FIGURE 2. ***In vivo* interaction between Dyrk1A and α-synuclein in rat brain and primary cortical neurons.** Whole brain tissue (*A*) or primary cortical neurons (*B*) were prepared from rat embryonic 17-day fetus. Whole cell lysates from rat brain (*A*) or primary cortical neurons (*B*) were immunoprecipitated (*IP*) with anti-α-synuclein or anti-Dyrk1A antibodies, followed by immunoblot analysis with anti-Dyrk1A or anti-α-synuclein antibodies, respectively. As a control, the cell extracts were immunoprecipitated with preimmune IgG (*IgG*) or empty protein A-beads (*Bead*). As an input control, α-synuclein and Dyrk1A expression was monitored by Western analysis. *C*, rat E17 cortical neurons were fixed, permeabilized, labeled subsequently with either anti-α-synuclein or anti-Dyrk1A antibodies, with fluorescein isothiocyanate- or rhodamine-attached secondary antibodies, and with 4′,6-diamidino-2-phenylindole. Immunostained preparations were examined using confocal microscopy. These results are representative of three independent experiments.

7.4). After reaction termination, the mixtures were analyzed by SDS-PAGE, and phosphorylated substrates were visualized by autoradiography.

Protein Aggregation Analysis—α-Synuclein aggregation was monitored with both turbidity and thioflavin-T binding fluorescence, as described previously (23). Purified α-synuclein samples were concentrated to 7 mg/ml using Centricon-3 spin filters (Amicon). After concentration, samples were centrifuged for 10 min at 100,000 × *g* to remove any aggregates that could have formed during the concentration step. The supernatants were adjusted to a final concentration of 7 mg/ml using Tris-buffered saline, 20 mM Tris, pH 7.5, and 0.2 M NaCl. Samples were dispensed into 1.5 ml of Beckman ultracentrifuge microtubes and incubated at 37 °C. At various time points, samples were centrifuged at 100,000 × *g* for 10 min, and supernatants were removed and diluted 10 times with Tris-buffered saline. These dilutions were analyzed by their absorbance at 280 nm. The remaining incubations were vortexed for 30 s to resuspend the pellets. For electron microscopy of α-synuclein aggregates, the samples were prepared as described previously (23). Samples were sectioned using an ultramicrotome, double-stained with uranyl acetate and lead citrate, and observed by transmission electron microscopy (Philips CM-10).

Construction of Dyrk1A siRNA Duplexes and Transfection—The competitive silencing and noncompetitive control Dyrk1A siRNAs were designed as reported by Sitz *et al.* (24) and provided by Sigma-Proligo (Boulder, CO). Dyrk1A siRNA duplexes were transfected into cells using the Lipofectamine Plus reagent according to the manufacturer's instructions.

RESULTS

Dyrk1A Binds to and Phosphorylates α-Synuclein in H19-7 Cells—We examined whether the α-synuclein and Dyrk1A interaction occurs in mammalian neuronal cells, such as in immortalized hippocampal H19-7 cells. We previously reported that the endogenous α-synuclein protein levels in H19-7 cells were undetectable (25, 26). Therefore, we transiently transfected H19-7 cells with α-synuclein cDNA, immunoprecipitated α-synuclein, and immunoblotted for Dyrk1A. Exogenously expressed α-synuclein binds to endogenous Dyrk1A (Fig. 1*A*). We confirmed this interaction by reverse co-immunoprecipitation and detecting the HA-tagged Dyrk1A-α-synuclein interaction in the dopaminergic neuroblastoma SH-SY5Y cell line (Fig. 1, *A* and *B*). These data demonstrate that α-synuclein interacts with Dyrk1A in H19-7 and SH-SY5Y cells.